

Estimating Treatment Effects with Independent Component Analysis

Patrik Reizinger^{*1,2}Lester Mackey³Wieland Brendel¹Rahul G. Krishnan^{2,4}¹Max Planck Institute for Intelligent Systems & ELLIS Institute, Tübingen, Germany²Vector Institute, Toronto, Canada³Microsoft Research, New England, USA⁴Department of Computer Science, University of Toronto, Toronto, Canada

Abstract

Independent Component Analysis (ICA) uses a measure of non-Gaussianity to identify latent sources from data and estimate their mixing coefficients [Shimizu et al., 2006]. Meanwhile, higher-order Orthogonal Machine Learning (OML) exploits non-Gaussian treatment noise to provide more accurate estimates of treatment effects in the presence of confounding nuisance effects [Mackey et al., 2018]. Remarkably, we find that the two approaches rely on the same moment conditions for consistent estimation. We then seize upon this connection to show how ICA can be effectively used for treatment effect estimation. Specifically, we prove that linear ICA can consistently estimate multiple treatment effects, even in the presence of Gaussian confounders, and identify regimes in which ICA is provably more sample-efficient than OML for treatment effect estimation. Our synthetic demand estimation experiments confirm this theory and demonstrate that linear ICA can accurately estimate treatment effects even in the presence of nonlinear nuisance.

1 INTRODUCTION

This work initiates the study of Independent Component Analysis (ICA) [Comon, 1994, Hyvärinen and Oja, 2000] for treatment effect estimation in the Partially Linear Regression (PLR) model [Robinson, 1988]. The accurate estimation of causal effects is a central challenge in medical research and policy-making [King, 1994], as it guides the development of more effective treatment strategies and interventions [Rosenbaum and Rubin, 1983, Pearl, 2009a,

Hill, 2011]. This task becomes difficult when the data contain high-dimensional confounding variables—features that affect both the treatment and the outcome. A number of machine learning methods have been developed to handle this setting while maintaining theoretical guarantees on treatment effect estimation. Among these methods, Orthogonal Machine Learning (OML) [Chernozhukov et al., 2017, Mackey et al., 2018, Jin et al., 2025] exhibits robust statistical properties in the PLR model [Robinson, 1988], where confounders affect the outcome and treatment in a potentially nonlinear way. OML’s two-stage procedure—first learning nuisance functions, then leveraging orthogonalization to adjust for confounders—yields consistent and efficient estimators of treatment effects under minimal assumptions.

ICA is a family of representation learning methods for separating mixed signals into statistically independent components, enabling the discovery of latent causal representations from observational data. While ICA is widely used for causal inference tasks [Tramontano et al., 2024, Khemakhem et al., 2021, Wendong et al., 2023], including linear [Shimizu et al., 2006] and nonlinear [Reizinger et al., 2023] Causal Discovery (CD), i.e., the extraction of a causal graph, the potential of ICA for treatment effect estimation is still underdeveloped. For example, the empirical studies of De Sousa Ribeiro et al. [2023], Jiang et al. [2023] employ nonlinear ICA for effect estimation but do not establish its consistency or analyze its estimation quality. Meanwhile, Shimizu et al. [2006] describe sufficient conditions for recovering the mixing matrix in linear ICA, but their assumptions are stronger than necessary, and they do not explore the important application of treatment effect estimation.

Interestingly, non-Gaussianity plays a crucial role in both ICA and treatment effect estimation. For (linear) ICA, non-Gaussianity is required to unambiguously disentangle the component sources, while, for treatment effect estimation, non-Gaussianity is required to achieve higher-order robustness in the PLR model [Mackey et al., 2018, Jin et al., 2025]. We seize upon this link and build upon the results

^{*}This work was initiated during P.R.’s internship at the Vector Institute. Correspondence to: patrik.reizinger@tuebingen.mpg.de

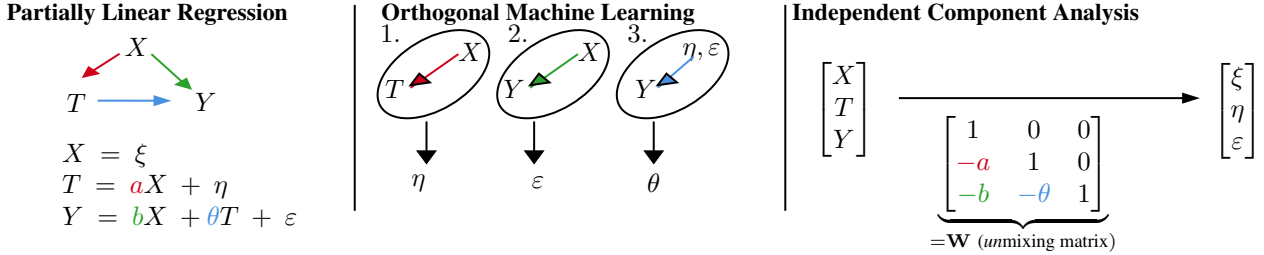


Figure 1: **Overview of treatment effect estimation in the Partially Linear Regression (PLR) model. (Left:)** The linear PLR model, where the covariates X affect both treatment T and outcome Y . The quantity of interest is the treatment effect θ . **(Center:)** Orthogonal Machine Learning (OML) estimates θ in three steps. **(Right:)** Independent Component Analysis (ICA) can invert the PLR model by maximizing non-Gaussianity of the sources, thereby yielding θ as a coefficient in the *unmixing matrix* \mathbf{W} . Scale and permutation indeterminacies are resolved by relying on non-Gaussianity and the PLR structure (Prop. 3.1).

of Shimizu et al. [2006], Mackey et al. [2018] to show that ICA can be used to effectively estimate treatment effects, both in theory and in practice. Focusing on the PLR model, we first prove that ICA can estimate treatment effects by reducing the problem to identifying the elements of the ICA unmixing matrix (cf. Fig. 1). Next, we show how the permutation and scale indeterminacies of ICA can be overcome by leveraging non-Gaussianity and the PLR structure. Remarkably, this construction enables effect estimation for multiple treatments and accommodates arbitrary (even Gaussian) covariate noise, all using the same off-the-shelf ICA algorithm, FastICA [Hyvarinen, 1999]. Experimentally, and perhaps surprisingly, we also demonstrate how to use *linear* ICA for estimating treatment effects in a nonlinear PLR. Our **primary contributions** can be summarized as follows:

- We formalize the link between Independent Component Analysis (ICA) and Orthogonal Machine Learning (OML) for PLR treatment effect estimation, clarifying the role of non-Gaussianity in both algorithms (§ 2.1) and identifying regimes in which each method is more sample efficient than the other (§ 3.2).
- We prove that ICA can be used to consistently estimate multiple treatment effects (Props. 3.1 and 3.2) and even effects with partially Gaussian source variables (Tab. 1 and Prop. 3.3).
- We complement our theory with a diversity of experiments simulating demand estimation from purchasing and pricing data; testing the effect of model coefficients on asymptotic variance; examining estimator performance under varying sample sizes, covariate dimensions, treatment dimensions, nonlinearities, and covariate noise distributions; and benchmarking the quality of linear ICA for non-linear treatment effect estimation (§ 4). In each case, ICA compares favorably with state-of-the-art OML approaches specifically developed for the PLR setting.

2 BACKGROUND

Partially Linear Regression (PLR). The PLR model of Robinson [1988] models the relationship between a scalar treatment T , a scalar outcome Y , and potentially confounding covariates X :

$$T = g(X) + \eta \text{ and } Y = \theta T + f(X) + \varepsilon \quad (1)$$

for independent (ε, η) with $\mathbb{E}[\varepsilon] = \mathbb{E}[\eta] = 0$.

Above, the coefficient θ is termed the *treatment effect*, f and g are nuisance functions capturing the influence of X , and ε and η are random noise variables.

Causality. Causality models cause and effect relationships as a Directed Acyclic Graph (DAG) between variables with functional relationships often specified by Structural Equation Models (SEMs) [Pearl, 2009b, Peters et al., 2018, Spirtes and Zhang, 2016]. A SEM consists of independent exogenous noise variables S (causes), dependent endogenous causal variables Z (effects), and functional mechanisms h describing the relationship between the variables, i.e., $Z_i \triangleq h_i(\text{Pa}(Z_i), S_i)$, where $\text{Pa}(Z_i)$ denotes the parent variables of Z_i in the graph. A special SEM family is that of Additive Noise Models (ANMs), where the exogenous variable S_i affects Z_i additively, i.e., $Z_i \triangleq h_i(\text{Pa}(Z_i)) + S_i$. Notably, as we illustrate in Fig. 1, the PLR model can be framed as an ANM with $Z = (X, Y, T)$ and $S = (\xi, \eta, \varepsilon)$ for $\xi \triangleq X$. We denote the covariate dimension by $d \triangleq \dim X$. We make the standard assumptions of no unobserved confounding and positivity, i.e., $\forall t : P(T = t | X) > 0$.

Independent Component Analysis (ICA). ICA models the observations as a deterministic mixture of *independent* sources [Comon, 1994, Hyvarinen et al., 2001]. The estimation goal for ICA is the recovery of the latent factors, and ICA provides identifiability guarantees for the factors in the infinite sample limit. Identifiability means that the ground-truth latent factors are recovered up to simple indeterminacies such as permutation and element-wise transformations. That is, for source variables S and observed mix-

tures $Z = \mathbf{A}S$, the objective of ICA is to recover $S = \mathbf{W}Z$, where \mathbf{A} is an unobserved *mixing matrix* and $\mathbf{W} \triangleq \mathbf{A}^{-1}$ is the *unmixing matrix*. Identifiability necessitates certain assumptions, even in the linear case, a central one being the non-Gaussianity of S . This can be seen, for example, by estimating the sources via maximizing the data log-likelihood, which is expressed in terms of the sources by the change-of-variables formula:

$$\log p_Z(Z) = \log p_S(S) + \log |\det \mathbf{W}|,$$

If more than one of the components of S is Gaussian, then rotating those sources does not change the likelihood. This is due to the rotation invariance of a Gaussian $p_S(S)$ and the fact that any orthogonal matrix \mathbf{O} preserves the absolute determinant, i.e., $|\det(\mathbf{W}\mathbf{O})| = |\det \mathbf{W} \det \mathbf{O}| = |\det \mathbf{W}|$ since $|\det \mathbf{O}| = 1$. Indeed, the goal of ICA is to find the most non-Gaussian directions in the data by maximizing a measure of non-Gaussianity. Common choices include maximizing the likelihood, maximizing kurtosis as in the original FastICA algorithm [Hyvärinen and Oja, 1997] (cf. Alg. 1), or maximizing negative entropy [Hyvärinen, 1997] or its approximation $\log \text{cosh}$ to minimize mutual information [Hyvärinen, 1999]. In each case, a different contrast function U is employed as a measure of non-Gaussianity (cf. § 3.2 for details).

Nonlinear ICA is usually impossible without further assumptions [Darmois, 1951, Hyvärinen and Pajunen, 1999, Locatello et al., 2019]. Recent developments have relaxed the independence condition to conditional independence and proved identifiability in the nonlinear case [Hyvärinen et al., 2019, Gresele et al., 2019, Khemakhem et al., 2020a, Hälvä et al., 2021, Hyvärinen and Morioka, 2016, Khemakhem et al., 2020b, Locatello et al., 2020, Morioka and Hyvärinen, 2023, Morioka et al., 2021, Reizinger et al., 2024b,a]. These methods often rely on data from multiple environments and require these environments to be “sufficiently diverse”. Examples include non-stationary time series or patient data collected at different hospitals with different socioeconomic and health statuses. The connection between ICA and Causal Discovery (CD) is well-known in the linear case of LiNGAM [Shimizu et al., 2006], and it was recently shown in the nonlinear case by Reizinger et al. [2023]. To the best of our knowledge, ICA has not been theoretically studied for treatment effect estimation, and this is the focus of the present work. Large- and finite-sample behavior of ICA estimators are also generally not the focus of identifiability research, though there exist several relevant results for the linear case [Herrmann and Theis, 2007, Bermejo, 2007, Auddy and Yuan, 2023].

Treatment Effect Estimation. Treatment effect estimation in the PLR model (1) focuses on the estimation of the coefficient θ . A wide variety of statistical methods have been developed for estimating treatment effects including Orthogonal Machine Learning (OML) [Chernozhukov et al., 2017,

Method	Reference	Noise	Output
OML	Chernozhukov et al. [2017]	any	$\hat{\theta}$
	Mackey et al. [2018]	non-G T	$\hat{\theta}\sqrt{n}$
ICA	Prop. 3.1	non-G	$\hat{\theta}, \hat{S}$
	Prop. 3.3	non-G $T \& Y$	$\hat{\theta}$

Table 1: **Assumptions for treatment effect estimation and source recovery under the PLR (equivalently, ANM) model.** G is shorthand for Gaussian, θ for the treatment effect with \sqrt{n} denoting improved estimation consistency, and S for the noise variables. $\hat{\cdot}$ indicates *estimated* quantities. ICA only uses the PLR structure for selecting the treatment effect coefficient from the unmixing matrix but not for source estimation.

Mackey et al., 2018, Jin et al., 2025], targeted maximum likelihood estimation [Schuler and Rose, 2017], propensity score-based techniques such as inverse probability of treatment weighting [Feng et al., 2012, McCaffrey et al., 2013], and Bayesian additive regression trees [Chipman et al., 2010], as well as extensions for multiple treatments [Hu et al., 2020, Xiang et al., 2025], high-dimensional and sparse treatments [Zhu et al., 2019], multi-level treatments [Xiao-chuan Shi and Wang, 2025], multiple heterogeneous environments [Kivva et al., 2025], and shared states [Hays and Raghavan, 2025].

Recently, Jin et al. [2025] showed that first-order OML [Chernozhukov et al., 2017] provides minimax rate-optimal treatment effect estimates when the PLR treatment noise is Gaussian and, surprisingly, that higher-order OML [Mackey et al., 2018] yields even higher quality estimates whenever the treatment noise is **not** Gaussian. Hence, while treatment effect estimation is still possible with Gaussian treatment noise, it is subject to a Gaussian quality barrier, reminiscent of the Gaussian identifiability barrier of ICA. We will next dig deeper into this connection and uncover a path toward ICA-based treatment effect estimation.

2.1 ROLE OF NON-GAUSSIANITY IN ICA AND OML

Linear ICA is impossible with more than one Gaussian source, as the rotational symmetry of the Gaussian distribution cannot be broken. If one makes additional assumptions, the causal graph can be recovered with more than one Gaussian source [Rolland et al., 2022, Montagna et al., 2023b]. However, even with Gaussian noise, consistent and asymptotically normal treatment effect estimation is possible with OML [Chernozhukov et al., 2017]. The difference enabling treatment effect estimation but not Blind Source Separation (BSS) is due to knowing the causal graph in treatment effect estimation: with a known causal graph, even the much harder Causal Representation Learning (CRL) problem be-

comes solvable under some circumstances [Wendong et al., 2023]. Knowing the causal graph translates into knowing the structure of the inverse map \mathbf{W} from observations to sources, i.e., knowing which elements are (non-)zero in \mathbf{W} , and this knowledge in turn breaks the rotational symmetry. Hence, there is no free lunch: the more relaxed conditions on the noise distribution come at the price of knowing the causal graph.

However, Mackey et al. [2018], Jin et al. [2025] showed that, even when one knows the causal graph, one can obtain more accurate and robust estimates of the treatment effect when the treatment noise is non-Gaussian. Hence, non-Gaussianity impacts not just infinite-sample consistency (the typical focus of ICA analyses) but also finite-sample estimator quality. These results can be intuitively summarized as non-Gaussian components are easier to discern, both in BSS and treatment effect estimation (cf. Tab. 1). In the sequel, we will exploit this connection to accurately estimate treatment effects with linear ICA.

3 ESTIMATING TREATMENT EFFECTS WITH ICA

Building on the insights of the preceding section, we now turn our attention to designing an ICA solution to the treatment effect estimation problem. Inverting the mixing function with ICA requires detailed knowledge of the data generating process (DGP), i.e., ICA needs to be able to extract the correct functional relationship up to an equivalence class. Shimizu et al. [2006], Reizinger et al. [2023] demonstrated that recovering the source variables conveys information about the causal structure. Treatment effect estimation, under the prevalent assumptions in the literature, presents a simpler task than recovering the source variables. Namely, it is only a partial reconstruction task (the target quantity is only the causal effect), with more prior knowledge (the causal graph is known). We will show how in this case, ICA can estimate treatment effects, even with Gaussian covariate noise.

Method summary. Operating under a linear additive model (Defn. 3.1), we use a two-step process to estimate the treatment effect with ICA (Fig. 1):

1. We run the FastICA algorithm to estimate the sources up to scaling and permutation.
2. We use our knowledge of the graph to resolve the permutation indeterminacy and the unit-variance of the outcome noise to resolve the scaling indeterminacy.

3.1 LINEAR PLR

We first prove that linear ICA can estimate treatment effects under a linear PLR model.

Definition 3.1 (Linear PLR). A linear PLR model with the graph $T \rightarrow Y$ and $T \leftarrow X \rightarrow Y$ and independent zero-mean sources (ξ, η, ε) has linear dependence on X given by the (inverse) SEM:

$$\begin{aligned} \begin{bmatrix} X \\ T \\ Y \end{bmatrix} &= \begin{bmatrix} 0 & 0 & 0 \\ a & 0 & 0 \\ b & \theta & 0 \end{bmatrix} \begin{bmatrix} X \\ T \\ Y \end{bmatrix} + \begin{bmatrix} \xi \\ \eta \\ \varepsilon \end{bmatrix} = \underbrace{\begin{bmatrix} 1 & 0 & 0 \\ a & 1 & 0 \\ b+a\theta & \theta & 1 \end{bmatrix}}_{=\mathbf{A} \text{ (mixing matrix)}} \begin{bmatrix} \xi \\ \eta \\ \varepsilon \end{bmatrix}, \\ \begin{bmatrix} \xi \\ \eta \\ \varepsilon \end{bmatrix} &= \underbrace{\begin{bmatrix} 1 & 0 & 0 \\ -a & 1 & 0 \\ -b & -\theta & 1 \end{bmatrix}}_{=\mathbf{W} \text{ (unmixing matrix)}} \begin{bmatrix} X \\ T \\ Y \end{bmatrix}. \end{aligned}$$

Shimizu et al. [2006] proved that linear ICA can be used for CD, where the unmixing matrix \mathbf{W} encodes the direct edges between (X, T, Y) —already highlighting the connection between the two fields. Under Assum. 3.1, linear ICA recovers the source variables up to scaling and permutation.

Assumption 3.1 (Linear ICA for PLR). In the linear PLR model of Defn. 3.1, we assume:

- (i) At most one of the source random variables (RVs) is Gaussian.
- (ii) There are no latent confounders.

However, source recovery alone is insufficient for treatment effect estimation, as linear ICA cannot resolve permutations and scaling. Fortunately, we can use our knowledge of the PLR causal graph to resolve the permutation [Reizinger et al., 2023]. Further, the canonical form of the ANM implies that the noise variables have a scalar factor of one [Hoyer et al., 2008], which means that we can resolve the scaling as well. We formalize these findings in the following result, proved in § C.1.

Proposition 3.1 (Treatment effect estimation with ICA). *When Assum. 3.1 holds and $\text{Var}(\varepsilon) = 1$, linear ICA identifies the causal effect θ at the global optimum of the loss in the infinite sample limit.*

Prop. 3.1 can be thought of as relaxing the assumptions and contextualizing the results of Shimizu et al. [2006] to show that ICA can be used to identify and consistently estimate treatment effects. This opens the door to new lines of inquiry connecting the well-developed methodology of ICA with the inferential goals of causal effect estimation.

3.2 FASTICA, OML, AND ASYMPTOTIC RELATIVE EFFICIENCY

As an initial case study, we next identify several similarities and differences between our ICA approach to PLR treatment effect estimation and the state-of-the-art OML approach.

When $\mathbb{E}[\eta^2] = 1$, both FastICA (Alg. 1) and higher-order OML employ a specific measure of non-Gaussianity U , like the excess kurtosis measure $U(\eta) = \eta^4 - 3$. FastICA uses U to identify non-Gaussian source variables, and, in our setting, Hyvarinen et al. [2001, Thm. 8.1] implies that FastICA consistently recovers the treatment noise source η if and only if

$$\mathbb{E}[\eta \cdot U'(\eta) - U''(\eta)] \neq 0. \quad (2)$$

Higher-order OML uses U to construct estimating equations that, remarkably, yield consistent, robust estimates of θ if and only if the same non-Gaussianity condition (2) is met [Mackey et al., 2018, Thm. 9]. For a detailed discussion, refer to § B. This correspondence allows us to provide a precise comparison between the asymptotic variances of the two treatment effect estimates when the same measure of non-Gaussianity is employed. See § C.3 for the proof of this result.

Theorem 3.1 (Asymptotic relative efficiency). *Under the assumptions of Auddy and Yuan [2023, Thm 4.5] and Mackey et al. [2018, Thm. 9] with $\text{Var}(\eta) = \text{Var}(\varepsilon) = 1$, the FastICA (Alg. 1) and higher-order OML treatment effect estimators with non-Gaussianity measure $U(\eta) = \eta^4 - 3$ are asymptotically normal with*

$$\text{AsymptoticVariance}(\hat{\theta}_{\text{OML}}) = \frac{\text{Var}(\eta^3) - 6\mathbb{E}[U(\eta)] - 9}{\mathbb{E}[U(\eta)]^2}, \quad (3)$$

$$\text{AsymptoticVariance}(\hat{\theta}_{\text{ICA}}) = \frac{((b+a\theta)^2 + 1)\text{Var}(\eta^3)}{\mathbb{E}[U(\eta)]^2}. \quad (4)$$

Remarkably, FastICA has smaller asymptotic variance—and hence higher sample efficiency—than the state-of-the-art OML estimator whenever the confounding effect $b + a\theta$ has small magnitude and the excess kurtosis $\mathbb{E}[U(\eta)]$ is sufficiently negative. Meanwhile, OML has smaller asymptotic variance when $(b + a\theta)^2$ or $\mathbb{E}[U(\eta)]$ is sufficiently large. In § 4.1, we will see these relative efficiencies reflected in our empirical results with FastICA dominating for smaller values of $(b + a\theta)^2$ and OML for larger.

3.3 ESTIMATING MULTIPLE TREATMENT EFFECTS

Next we show that ICA can be used to simultaneously estimate the effects of multiple treatments. For illustration, we consider two treatments:

Definition 3.2 (Multiple treatment linear PLR). A linear PLR model with the graph $T_1 \rightarrow Y$, $T_2 \rightarrow Y$, and $T_{1,2} \leftarrow X \rightarrow Y$ and independent zero-mean $(\xi, \eta_1, \eta_2, \varepsilon)$ is

given by the (inverse) SEM:

$$\begin{bmatrix} X \\ T_1 \\ T_2 \\ Y \end{bmatrix} = \begin{bmatrix} 0 & 0 & 0 & 0 \\ a_1 & 0 & 0 & 0 \\ a_2 & 0 & 0 & 0 \\ b & \theta_1 & \theta_2 & 0 \end{bmatrix} \begin{bmatrix} X \\ T_1 \\ T_2 \\ Y \end{bmatrix} + \begin{bmatrix} \xi \\ \eta_1 \\ \eta_2 \\ \varepsilon \end{bmatrix},$$

$$\begin{bmatrix} \xi \\ \eta_1 \\ \eta_2 \\ \varepsilon \end{bmatrix} = \begin{bmatrix} 1 & 0 & 0 & 0 \\ -a_1 & 1 & 0 & 0 \\ -a_2 & 0 & 1 & 0 \\ -b & -\theta_1 & -\theta_2 & 1 \end{bmatrix} \begin{bmatrix} X \\ T_1 \\ T_2 \\ Y \end{bmatrix}.$$

Proposition 3.2 (Estimating multiple treatment effects with ICA). *Under Assum. 3.1 in the multiple treatment linear PLR model (Defn. 3.2), ICA identifies all treatment effects at the global optimum of the loss in the infinite sample limit.*

The proof in § C.2 parallels that for single treatments.

3.4 TOLERATING GAUSSIAN COVARIATES

Our next result shows that, perhaps surprisingly, ICA can accurately identify treatment effects even when one or more covariates are Gaussian. This result, proved in § C.4, still uses the non-Gaussianity of both the outcome and treatment noise to distinguish the nuisance effects.

Proposition 3.3 (Treatment effect estimation with Gaussian covariates and ICA). *Consider the generalization of the linear PLR model (Defn. 3.1) with d covariates X . If $\text{Var}(\varepsilon) = 1$ and both ε and η are non-Gaussian, then linear ICA identifies the treatment effect at the global optimum of the loss in the infinite data limit (even if one or more covariates are Gaussian).*

3.5 TREATMENT EFFECT ESTIMATION UNDER MODEL MISSPECIFICATION: NONLINEAR PLR

We next investigate the case when the covariates affect treatment and outcome in a nonlinear way. Specifically, we will use insights from the fields of nonlinear ICA (conditional independence) and score-based CD (derivatives for ANMs, deferred to § A) to assess the feasibility of using FastICA—which operates under a linear ICA model—for treatment effect estimation in the nonlinear PLR model.

Definition 3.3 (Nonlinear PLR). A nonlinear PLR model with the graph $T \rightarrow Y$ and $T \leftarrow X \rightarrow Y$ and independent zero-mean (ξ, η, ε) is given by the (inverse) SEM:

$$\begin{bmatrix} X \\ T \\ Y \end{bmatrix} = \begin{bmatrix} \xi \\ g(X) + \eta \\ f(X) + \theta T + \varepsilon \end{bmatrix}; \quad \begin{bmatrix} \xi \\ \eta \\ \varepsilon \end{bmatrix} = \begin{bmatrix} X \\ T - g(X) \\ Y - f(X) - \theta T \end{bmatrix}.$$

Insights from nonlinear ICA: conditional independencies in PLR. Many nonlinear ICA methods assume a notion of “variability” of the data distribution, which can often be characterized by additional conditional independencies [Guo et al., 2022, 2024, Reizinger et al., 2024b]. Inspired by these results, we apply the lens of conditional independence to the PLR model. By introducing two conditional source variables $\varepsilon'(X), \eta'(X)$ —where X plays the role of the auxiliary variable in the nonlinear ICA literature—we can rewrite the nonlinear PLR equations into a form which shows their conditional independence given X :

$$\varepsilon'(X) = f(X) + \varepsilon; \quad \eta'(X) = g(X) + \eta; \quad (5)$$

$$\eta'(X) \perp\!\!\!\perp \varepsilon'(X) \mid X. \quad (6)$$

As the above conditional independence does not depend on the distribution of X , as in Prop. 3.3, X can even have a Gaussian distribution. Moreover, this nonlinear, conditionally independent setup is known to yield identifiability under “sufficient variability conditions” that arise, for example, when data are generated from sufficiently different subgroups [Hyvarinen and Morioka, 2016, Hyvarinen et al., 2019, Wendong et al., 2023, Reizinger et al., 2024b, Morioka and Hyvarinen, 2023]. When the identifiability result is up to permutation, scaling, and zero-preserving elementwise nonlinear transformations, then we can recover the causal graph and resolve the permutation indeterminacy by the result of Reizinger et al. [2023]. When we have identifiability up to only permutation and scaling, we recover the following Jacobian of the inference map from Z to S up to a non-zero constant c :

$$\mathbf{J} = c \cdot \begin{bmatrix} 1 & 0 & 0 \\ -g'(X) & 1 & 0 \\ -f'(X) & -\theta & 1 \end{bmatrix}. \quad (7)$$

Fortunately, due to the specific additive structure of the PLR model, we can also recover the treatment effect exactly from this scaled Jacobian by simply dividing the $-\theta$ entry of the Jacobian by any diagonal entry to eliminate the unknown scaling.

Using FastICA for nonlinear PLR. The above intuition gives us hope that if we only aim to selectively estimate the treatment effect (and not to solve the full BSS problem), then the additive structure of PLR might lead to good treatment effect estimates, even when the covariates affect both treatment and outcome nonlinearly. We explicitly test this using the following setup, cf. § 4.2):

1. We generate data from a nonlinear PLR model;
2. We input the observations, i.e., (X, T, Y) into *linear* FastICA; and
3. We use the same strategy as in Prop. 3.1 to resolve the permutation and scaling indeterminacies.

4 EXPERIMENTS

We now turn to an empirical evaluation to validate the insights from our theory. We ground our analysis in the demand estimation setting of Mackey et al. [2018] and provide open-source Python code replicating all experiments.¹

4.1 DEMAND ESTIMATION FROM PRICE AND PURCHASE DATA

While the partially linear and non-Gaussian assumptions of this work are by no means universal, there are many practical inference scenarios in which both are known to hold. One important example detailed in Mackey et al. [2018] is demand estimation from purchasing and pricing data. In this setting, the outcome Y is the observed demand for a product, the treatment T is the price of that product, and, commonly, conditional on all observable covariates X , the treatment noise follows a discrete (and non-Gaussian) distribution representing random discounts offered to customers over a baseline price linear $g(X)$ in the observable variables.

Assessing relative efficiency. To validate the relative efficiency theory of Thm. 3.1, we will compare our FastICA-based effect estimation strategy with the state-of-the-art higher-order OML [Mackey et al., 2018] method. We begin by replicating the synthetic demand estimation experiments of Mackey et al. [2018, Sec. 5] with $n = 5000$, $d = 10$, uniform and unit-variance ε , discrete η , independent generalized-normal covariates X with $\beta = 1$, varying $\theta \in \{0.01, 0.1, 0.5, 1, 3, 10\}$, and varying sparse linear $f(x)$ and $g(x)$ with $s = 1$ non-zero coefficient $a \in \{-0.002, 0.05, -0.43, 1.56\}$ and $b \in \{0.003, -0.02, 0.63, -1.45\}$. We use the `scikit-learn` [Pedregosa et al., 2011] implementation of FastICA with a `logcosh` loss function and `unit-variance` whitening. We use the implementation of Mackey et al. [2018] for OML methods and use the same tolerance (10^{-4}) and iteration count (1000) for all methods.

Results. As Thm. 3.1 characterizes the regimes in which either FastICA or OML is more sample efficient, we focus on comparing the estimators’ relative efficiency here and include absolute performance metrics and extensive ablations in § E. Fig. 2 shows that ICA’s relative performance depends on the asymptotic variance coefficient $c_{\text{ICA}} \triangleq 1 + |b + a\theta|_2^2$ derived in Thm. 3.1. Namely, ICA dominates when the asymptotic variance coefficient $c_{\text{ICA}} < 1.5$ (96.3% win rate) and overall (72.9% win rate), while OML is preferable in the medium regime ($1.5 \leq c_{\text{ICA}} < 5$), winning 64.3% of configurations.

Ablations over n , d , and β . When $c_{\text{ICA}} < 1.5$, we further find that ICA outperforms OML across nearly all tested sam-

¹Code: github.com/rpatrik96/ica_causal_effect.

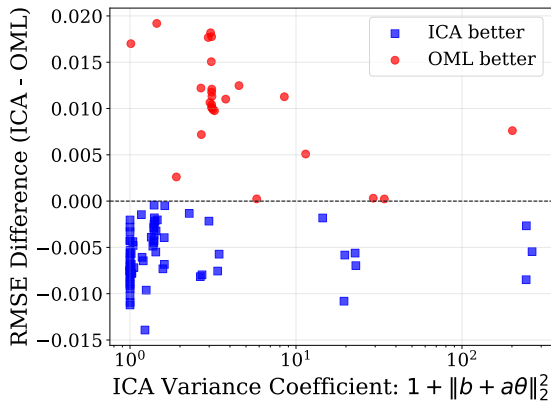


Figure 2: **Relative efficiency of ICA vs. higher-order OML for demand estimation** (see § 4.1). **Left:** RMSE difference (ICA – OML) as a function of the ICA asymptotic variance coefficient $c_{ICA} = 1 + (b + a\theta)^2$ derived in [Thm. 3.1](#). Blue points indicate ICA outperforms OML; red points indicate OML outperforms ICA. **Right:** Performance stratified by c_{ICA} regime. ICA wins overall (72.9% win rate), dominating especially when $c_{ICA} < 1.5$ (96.3% win rate). OML is preferable in the medium regime ($1.5 \leq c_{ICA} < 5$), with a 64.3% win rate.

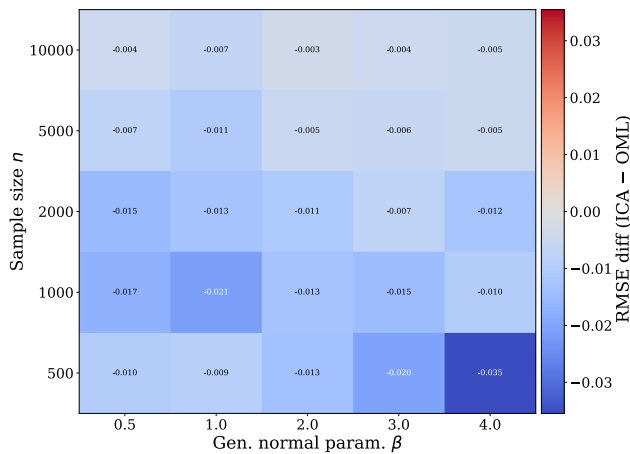


Figure 3: **RMSE difference (ICA – higher-order OML) as n and covariate distribution β vary** for $c_{ICA} < 1.5$.

ple sizes $n \in \{100, 200, 500, 1000, 2000, 5000\}$, covariate dimension $d \in \{2, 5, 10, 20, 50\}$, and covariate distributions, with the advantage being most pronounced for small sample sizes, higher values of the generalized normal parameter β (i.e., for negative excess kurtosis, or equivalently, thinner tails), and lower covariate dimension (see [Figs. 3](#) and [E.3](#) for RMSE and bias difference heatmaps across these dimensions). Even more surprisingly, ICA can comparably or better estimate the treatment effect even if the noises are Gaussian, that is, when source identification is impossible ([Fig. E.3](#), right column, $\beta = 2$). We report the Mean Correlation Coefficient (MCC) [[Hyvarinen and Morioka, 2016](#)], a measure of source identification in [Fig. E.1](#), demonstrating that low MCC values for Gaussian sources do not prohibit treatment effect estimation. The absolute MSE values for ICA are shown in [Fig. E.2](#). These empirical findings align with our asymptotic relative efficiency analysis ([Thm. 3.1](#)):

ICA is more accurate than OML when the confounding effect ($b + a\theta$) is smaller in magnitude.

Additional ablations. We present additional ablations varying a , b , θ , and c_{ICA} in [Fig. E.9](#) and [Tab. E.3](#), varying the FastICA loss function in [Fig. E.16](#), and varying the treatment noise η distribution and variance in [Figs. E.4, E.5](#) and [E.8](#). Notably, we find in [Fig. E.5](#) that ICA continues to outperform OML across a wide range of treatment distributions with varying kurtoses including discrete, Laplace, Uniform, and Rademacher.

4.2 LINEAR ICA FOR NONLINEAR PLR

Setup. We next assess the accuracy of linear ICA for treatment effect estimation in the nonlinear PLR model of [Defn. 3.3](#). We fix $n = 5000$ and $\theta = 1.55$, use Laplace noise (with location 0 and scale 1) for ε , η , and X , vary the covariate dimension $d \in \{2, 5, 10, 20, 50\}$ and consider four nonlinearities ϕ for the nuisance functions $f(x) = \phi(\langle w, x \rangle)$ and $g(x) = \phi(\langle v, x \rangle)$, where ϕ is selected from a rectified linear unit (ReLU), a leaky ReLU (with slope 0.2), a sigmoid, and tanh. Unlike the single non-zero entry per coefficient vector in § 4.1, the treatment coefficient vector a has approximately 30% non-zero entries and the outcome coefficient vector b is fully dense, both drawn from $\mathcal{N}(0, 1)$. We use the same FastICA configuration (logcosh, unit-variance whitening) as in § 4.1. We ablate over the value of θ , the slope of the leaky ReLU, the sparsity of the mixing matrix, and the noise density by changing the generalized normal density’s β parameter ($\beta = 1$ is Laplace) in § E.

Results. In [Fig. 4](#) (left) we report the mean squared relative error, i.e., $|(\theta - \hat{\theta})/\theta|$, of FastICA across 20 random seeds. Remarkably, linear FastICA performs very well even

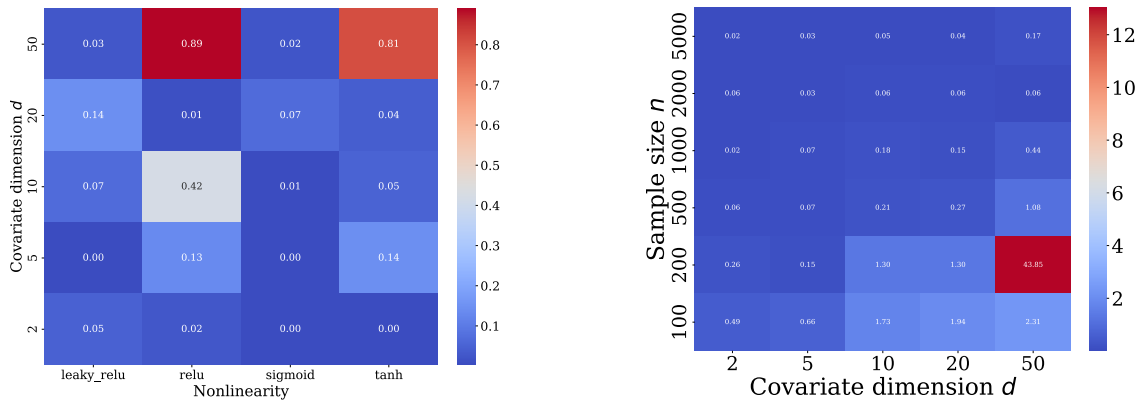


Figure 4: **Left:** Relative Mean Squared Error (MSE) of treatment effect estimation for Laplace noises in *nonlinear* PLR across multiple covariate dimensions for *linear* ICA with different nonlinearities with 5,000 samples. Leaky ReLU uses a slope of 0.2. See Fig. E.12 for an ablation over slopes. **Right:** Relative MSE of ICA treatment effect estimation across covariate dimensions d and sample sizes n for $m = 2$ treatments in linear PLR. Means calculated from 20 seeds. See Fig. E.15 for an ablation over treatment counts.

under model misspecification. That is, it exhibits low relative mean squared error in treatment effect estimation with relative error below 5% in most scenarios. While we do not have a precise theory to characterize success within the nonlinear regime, our empirical results showcase promise. In Figs. E.10 to E.12, we perform additional ablations over the location and scale parameters of the generalized normal distribution, and leaky ReLU slopes, observing comparable performance in most settings. Performance is rather insensitive to location and scale (relative error is in the 4 – 8% range), β has the same effect as in the linear case (cf. Fig. E.11 left and right), with the highest mean relative errors occurring when $\beta \in \{2, 2.5, 3\}$, i.e., when the densities are (close to) Gaussian—which is $\beta = 2$. Perhaps surprisingly, when only the covariates are Gaussian, we achieve lower relative estimation error than when every noise is Laplace. Fig. E.13 provides a comprehensive view of the robustness across dimensions and nonlinearity types, while Fig. E.14 shows the effect of Gaussian covariates and different treatment effect sampling strategies.

4.3 ESTIMATING MULTIPLE TREATMENT EFFECTS

Setup. Finally, we evaluate the effectiveness of ICA for simultaneously estimating multiple treatment effects as in Defn. 3.2, a question that, to the best of our knowledge, has not seen much work using estimators based on higher-order OML. We use the first m treatment effects in the array $\theta = [1.55, 0.65, -2.45, 1.75, -1.35]$ for $m \in \{1, 2, 5\}$ and otherwise adopt the setup of § 4.2.

Results. Fig. 4 (right) reports the mean squared relative error $\|(\theta - \hat{\theta})/\theta\|_2$ across 20 random seeds for $d = 10$. Our primary finding is that when samples are abundant, ICA remains a stable and high-quality estimator across multiple

treatments; however the quality of the estimator degrades as a function of m when samples are scarce. Additional experiments ablating the covariate dimension can be found in Fig. E.15.

5 DISCUSSION, LIMITATIONS, AND FUTURE WORK

This work initiated the study of Independent Component Analysis (ICA) for treatment effect estimation, focusing on the Partially Linear Regression (PLR) model and forging connections with the state-of-the-art higher-order Orthogonal Machine Learning (OML) approach of Mackey et al. [2018].

We theoretically characterized how ICA can consistently estimate single or multiple treatment effects (Props. 3.1 and 3.2) and how the ubiquitous non-Gaussianity assumption in ICA can be relaxed for the covariate noises (Prop. 3.3). We further demonstrated empirically that linear ICA can accurately estimate treatment effects even in the presence of nonlinear nuisance effects (§ 4.2). Finally, we related the asymptotic variances for ICA and OML and identified regimes in which ICA is provably more sample efficient and empirically more accurate.

This work also has its limitations, pointing to several important directions for future work including (1) developing a complete theory of linear ICA for nonlinear PLR, (2) studying the robustness of ICA treatment effect estimates to inaccuracies in estimated nuisance effects, and (3) developing ICA-based tools for causal effect estimation beyond the PLR model. In § E.9, we also compare FastICA with DirectLiNGAM [Shimizu et al., 2011], finding complementary strengths: DirectLiNGAM excels in low-dimensional dense settings ($d \leq 10$), while FastICA is preferable for

sparse, high-dimensional ($d \geq 20$), or heavily non-Gaussian data.

Author Contributions

P.R. conceived the idea, developed the theory, implemented the experiments, and wrote the paper. L.M. provided guidance on the theoretical analysis and OML methodology. W.B. and R.G.K. supervised the project and provided feedback.

Acknowledgements

The authors thank Vahid Balazadeh for his insightful comments. Patrik Reizinger acknowledges his membership in the European Laboratory for Learning and Intelligent Systems (ELLIS) PhD program and thanks the International Max Planck Research School for Intelligent Systems (IMPRS-IS) for its support. This work was supported by the German Federal Ministry of Education and Research (BMBF): Tübingen AI Center, FKZ: 01IS18039A. Wieland Brendel acknowledges financial support via an Emmy Noether Grant funded by the German Research Foundation (DFG) under grant no. BR 6382/1-1 and via the Open Philanthropy Foundation funded by the Good Ventures Foundation. Wieland Brendel is a member of the Machine Learning Cluster of Excellence, EXC number 2064/1 – Project number 390727645. This research utilized compute resources at the Tübingen Machine Learning Cloud, DFG FKZ INST 37/1057-1 FUGG.

References

Arnab Auddy and Ming Yuan. Large Dimensional Independent Component Analysis: Statistical Optimality and Computational Tractability, March 2023. URL <http://arxiv.org/abs/2303.18156>. arXiv:2303.18156 [math].

Sergio Bermejo. Finite sample effects of the fast ICA algorithm. *Neurocomputing*, 71(1-3): 392–399, December 2007. ISSN 09252312. doi: 10.1016/j.neucom.2006.09.015. URL <https://linkinghub.elsevier.com/retrieve/pii/S0925231207000203>.

Victor Chernozhukov, Denis Chetverikov, Mert Demirer, Esther Duflo, Christian Hansen, Whitney Newey, and James Robins. Double/Debiased Machine Learning for Treatment and Causal Parameters, December 2017. URL <http://arxiv.org/abs/1608.00060>. arXiv:1608.00060 [econ, stat].

Hugh A. Chipman, Edward I. George, and Robert E. McCulloch. BART: Bayesian additive regression trees. *The Annals of Applied Statistics*, 4(1):

266–298, March 2010. ISSN 1932-6157, 1941-7330. doi: 10.1214/09-AOAS285. URL <https://projecteuclid.org/journals/annals-of-applied-statistics/volume-4/issue-1/BART-Bayesian-additive-regression-trees/10.1214/09-AOAS285.full>. Publisher: Institute of Mathematical Statistics.

Pierre Comon. Independent component analysis, a new concept? *Signal processing*, 36(3):287–314, 1994. doi: 10.1016/0165-1684(94)90029-9. URL [https://doi.org/10.1016/0165-1684\(94\)90029-9](https://doi.org/10.1016/0165-1684(94)90029-9).

George Darmais. Analyse des liaisons de probabilité. In *Proc. Int. Stat. Conferences 1947*, page 231, 1951.

Fabio De Sousa Ribeiro, Tian Xia, Miguel Monteiro, Nick Pawlowski, and Ben Glocker. High fidelity image counterfactuals with probabilistic causal models. In Andreas Krause, Emma Brunskill, Kyunghyun Cho, Barbara Engelhardt, Sivan Sabato, and Jonathan Scarlett, editors, *Proceedings of the 40th International Conference on Machine Learning*, volume 202 of *Proceedings of Machine Learning Research*, pages 7390–7425. PMLR, 23–29 Jul 2023. URL <https://proceedings.mlr.press/v202/de-sousa-ribeiro23a.html>.

Ping Feng, Xiao-Hua Zhou, Qing-Ming Zou, Ming-Yu Fan, and Xiao-Song Li. Generalized propensity score for estimating the average treatment effect of multiple treatments. *Statistics in Medicine*, 31(7):681–697, 2012. ISSN 1097-0258. doi: 10.1002/sim.4168. URL <https://onlinelibrary.wiley.com/doi/abs/10.1002/sim.4168>. [_eprint: https://onlinelibrary.wiley.com/doi/pdf/10.1002/sim.4168](https://onlinelibrary.wiley.com/doi/pdf/10.1002/sim.4168).

Luigi Gresele, Paul K. Rubenstein, Arash Mehrjou, Francesco Locatello, and Bernhard Schölkopf. The Incomplete Rosetta Stone Problem: Identifiability Results for Multi-View Nonlinear ICA. *arXiv:1905.06642 [cs, stat]*, pages 217–227, August 2019. URL <http://arxiv.org/abs/1905.06642>. arXiv: 1905.06642.

Siyuan Guo, Viktor Tóth, Bernhard Schölkopf, and Ferenc Huszár. Causal de Finetti: On the Identification of Invariant Causal Structure in Exchangeable Data. *arXiv:2203.15756 [cs, math, stat]*, March 2022. URL <http://arxiv.org/abs/2203.15756>. arXiv: 2203.15756.

Siyuan Guo, Chi Zhang, Karthika Mohan, Ferenc Huszár, and Bernhard Schölkopf. Do Finetti: On Causal Effects for Exchangeable Data, May 2024. URL <http://arxiv.org/abs/2405.18836>. arXiv:2405.18836 [cs, stat].

Chris Hays and Manish Raghavan. Double Machine Learning for Causal Inference under Shared-State Interfer-

- ence, April 2025. URL <http://arxiv.org/abs/2504.08836>. arXiv:2504.08836 [stat].
- J. Michael Herrmann and Fabian J. Theis. Statistical Analysis of Sample-Size Effects in ICA. In Hujun Yin, Peter Tino, Emilio Corchado, Will Byrne, and Xin Yao, editors, *Intelligent Data Engineering and Automated Learning - IDEAL 2007*, volume 4881, pages 416–425. Springer Berlin Heidelberg, Berlin, Heidelberg, 2007. ISBN 978-3-540-77225-5. doi: 10.1007/978-3-540-77226-2_43. URL http://link.springer.com/10.1007/978-3-540-77226-2_43. Series Title: Lecture Notes in Computer Science.
- Jennifer L Hill. Bayesian nonparametric modeling for causal inference. *Journal of Computational and Graphical Statistics*, 20(1):217–240, 2011. doi: 10.1198/jcgs.2010.08162. URL <https://doi.org/10.1198/jcgs.2010.08162>.
- Patrik Hoyer, Dominik Janzing, Joris M Mooij, Jonas Peters, and Bernhard Schölkopf. Nonlinear causal discovery with additive noise models. In *Advances in Neural Information Processing Systems*, volume 21, pages 689–696. Curran Associates, Inc., 2008. URL <https://proceedings.neurips.cc/paper/2008/hash/f7664060cc52bc6f3d620bcdec94a4b6-Abstract.html>.
- Liangyuan Hu, Chenyang Gu, Michael Lopez, Jiayi Ji, and Juan Wisnivesky. Estimation of causal effects of multiple treatments in observational studies with a binary outcome. *Statistical Methods in Medical Research*, 29(11):3218–3234, November 2020. ISSN 0962-2802. doi: 10.1177/0962280220921909. URL <https://www.ncbi.nlm.nih.gov/pmc/articles/PMC7534201/>.
- Aapo Hyvärinen. New approximations of differential entropy for independent component analysis and projection pursuit. *Advances in neural information processing systems*, 10, 1997.
- Aapo Hyvärinen. Fast and robust fixed-point algorithms for independent component analysis. *IEEE transactions on Neural Networks*, 10(3):626–634, 1999. doi: 10.1109/72.761722. URL <https://doi.org/10.1109/72.761722>.
- Aapo Hyvärinen and Hiroshi Morioka. Unsupervised Feature Extraction by Time-Contrastive Learning and Nonlinear ICA. *arXiv:1605.06336 [cs, stat]*, May 2016. URL <http://arxiv.org/abs/1605.06336>. arXiv: 1605.06336.
- Aapo Hyvärinen and Erkki Oja. A fast fixed-point algorithm for independent component analysis. *Neural computation*, 9(7):1483–1492, 1997.
- Aapo Hyvärinen, Juha Karhunen, and Erkki Oja. *Independent component analysis*. J. Wiley, New York, 2001. ISBN 978-0-471-40540-5.
- Aapo Hyvärinen, Hiroaki Sasaki, and Richard E. Turner. Nonlinear ICA Using Auxiliary Variables and Generalized Contrastive Learning. *arXiv:1805.08651 [cs, stat]*, pages 859–868, February 2019. URL <http://arxiv.org/abs/1805.08651>. arXiv: 1805.08651.
- A. Hyvärinen and E. Oja. Independent component analysis: algorithms and applications. *Neural Networks*, 13(4):411–430, June 2000. ISSN 0893-6080. doi: 10.1016/S0893-6080(00)00026-5. URL <https://www.sciencedirect.com/science/article/pii/S0893608000000265>.
- Aapo Hyvärinen and Petteri Pajunen. Nonlinear independent component analysis: Existence and uniqueness results. *Neural Networks*, 12(3):429–439, April 1999. ISSN 0893-6080. doi: 10.1016/S0893-6080(98)00140-3. URL <https://www.sciencedirect.com/science/article/pii/S0893608098001403>.
- Hermanni Hälvä, Sylvain Le Corff, Luc Lehéricy, Jonathan So, Yongjie Zhu, Elisabeth Gassiat, and Aapo Hyvärinen. Disentangling Identifiable Features from Noisy Data with Structured Nonlinear ICA. *arXiv:2106.09620 [cs, stat]*, June 2021. URL <http://arxiv.org/abs/2106.09620>. arXiv: 2106.09620.
- Ziyang Jiang, Yiling Liu, Michael H Klein, Ahmed Aloui, Yiman Ren, Keyu Li, Vahid Tarokh, and David Carlson. Causal mediation analysis with multi-dimensional and indirectly observed mediators. *arXiv preprint arXiv:2306.07918*, abs/2306.07918, 2023. doi: 10.48550/arxiv.2306.07918. URL <https://doi.org/10.48550/arXiv.2306.07918>.
- Jikai Jin, Lester Mackey, and Vasilis Syrgkanis. It’s hard to be normal: The impact of noise on structure-agnostic estimation. *arXiv preprint arXiv:2507.02275*, abs/2507.02275, 2025. doi: 10.48550/arxiv.2507.02275. URL <https://doi.org/10.48550/arXiv.2507.02275>.
- Ilyes Khemakhem, Diederik Kingma, Ricardo Monti, and Aapo Hyvärinen. Variational Autoencoders and Nonlinear ICA: A Unifying Framework. In *International Conference on Artificial Intelligence and Statistics*, pages 2207–2217. PMLR, June 2020a. URL <http://proceedings.mlr.press/v108/khemakhem20a.html>. ISSN: 2640-3498.
- Ilyes Khemakhem, Ricardo Pio Monti, Diederik P. Kingma, and Aapo Hyvärinen. ICE-BeeM: Identifiable Conditional Energy-Based Deep Models Based on Nonlinear ICA. *arXiv:2002.11537 [cs, stat]*, October 2020b. URL

- <http://arxiv.org/abs/2002.11537>. arXiv:2002.11537.
- Ilyes Khemakhem, Ricardo Pio Monti, Robert Leech, and Aapo Hyvärinen. Causal Autoregressive Flows. *arXiv:2011.02268 [cs, stat]*, pages 3520–3528, February 2021. URL <http://arxiv.org/abs/2011.02268>. arXiv:2011.02268.
- Gary King. Designing social inquiry: Scientific inference in qualitative research, 1994.
- Yaroslav Kivva, Sina Akbari, Saber Salehkaleybar, and Negar Kiyavash. Causal Effect Identification in Heterogeneous Environments from Higher-Order Moments, June 2025. URL <http://arxiv.org/abs/2506.11756>. arXiv:2506.11756 [cs].
- Francesco Locatello, Stefan Bauer, Mario Lucic, Gunnar Raetsch, Sylvain Gelly, Bernhard Schölkopf, and Olivier Bachem. Challenging Common Assumptions in the Unsupervised Learning of Disentangled Representations. In *International Conference on Machine Learning*, pages 4114–4124. PMLR, May 2019. doi: 10.1609/aaai.v34i09.7120. URL <http://proceedings.mlr.press/v97/locatello19a.html>. ISSN: 2640-3498.
- Francesco Locatello, Ben Poole, Gunnar Rätsch, Bernhard Schölkopf, Olivier Bachem, and Michael Tschanen. Weakly-Supervised Disentanglement Without Compromises. *arXiv:2002.02886 [cs, stat]*, pages 6348–6359, October 2020. URL <http://arxiv.org/abs/2002.02886>. arXiv:2002.02886.
- Lester Mackey, Vasilis Syrgkanis, and Ilias Zadik. Orthogonal machine learning: Power and limitations. In Jennifer Dy and Andreas Krause, editors, *Proceedings of the 35th International Conference on Machine Learning*, volume 80 of *Proceedings of Machine Learning Research*, pages 3375–3383. PMLR, 10–15 Jul 2018. URL <https://proceedings.mlr.press/v80/mackey18a.html>.
- Daniel F. McCaffrey, Beth Ann Griffin, Daniel Almirall, Mary Ellen Slaughter, Rajeev Ramchand, and Lane F. Burgette. A tutorial on propensity score estimation for multiple treatments using generalized boosted models. *Statistics in Medicine*, 32(19):3388–3414, 2013. ISSN 1097-0258. doi: 10.1002/sim.5753. URL <https://onlinelibrary.wiley.com/doi/abs/10.1002/sim.5753>. eprint: <https://onlinelibrary.wiley.com/doi/pdf/10.1002/sim.5753>.
- Francesco Montagna, Nicoletta Noceti, Lorenzo Rosasco, Kun Zhang, and Francesco Locatello. Causal Discovery with Score Matching on Additive Models with Arbitrary Noise, April 2023a. URL <http://arxiv.org/abs/2304.03265>. arXiv:2304.03265 [cs, stat].
- Francesco Montagna, Nicoletta Noceti, Lorenzo Rosasco, Kun Zhang, and Francesco Locatello. Scalable Causal Discovery with Score Matching, April 2023b. URL <http://arxiv.org/abs/2304.03382>. arXiv:2304.03382 [cs, stat].
- Francesco Montagna, Philipp M. Faller, Patrick Bloebaum, Elke Kirschbaum, and Francesco Locatello. Score matching through the roof: linear, nonlinear, and latent variables causal discovery, July 2024. URL <http://arxiv.org/abs/2407.18755>. arXiv:2407.18755 [cs, stat].
- Hiroshi Morioka and Aapo Hyvärinen. Connectivity-contrastive learning: Combining causal discovery and representation learning for multimodal data. In *Proceedings of The 26th International Conference on Artificial Intelligence and Statistics*, pages 3399–3426. PMLR, April 2023. URL <https://proceedings.mlr.press/v206/morioka23a.html>. ISSN: 2640-3498.
- Hiroshi Morioka, Hermanni Hälvä, and Aapo Hyvärinen. Independent Innovation Analysis for Nonlinear Vector Autoregressive Process. *arXiv:2006.10944 [cs, stat]*, February 2021. URL <https://arxiv.org/abs/2006.10944>. arXiv:2006.10944.
- Judea Pearl. Causal inference in statistics: An overview. *Statistics Surveys*, 3(none), 2009a. doi: 10.1214/09-ss057. URL <https://doi.org/10.1214/09-ss057>.
- Judea Pearl. *Causality: Models, Reasoning, and Inference*, volume 110. Cambridge University Press, Cambridge, 2 edition, 2009b. ISBN 978-0-511-80316-1. doi: 10.1017/CBO9780511803161. URL <http://ebooks.cambridge.org/ref/id/CBO9780511803161>.
- F. Pedregosa, G. Varoquaux, A. Gramfort, V. Michel, B. Thirion, O. Grisel, M. Blondel, P. Prettenhofer, R. Weiss, V. Dubourg, J. Vanderplas, A. Passos, D. Cournapeau, M. Brucher, M. Perrot, and E. Duchesnay. Scikit-learn: Machine learning in Python. *Journal of Machine Learning Research*, 12:2825–2830, 2011. doi: 10.5555/1953048.2078195. URL <https://dl.acm.org/doi/10.5555/1953048.2078195>.
- Jonas Peters, Dominik Janzing, and Bernhard Schölkopf. Elements of causal inference: foundations and learning algorithms. *Journal of Statistical Computation and Simulation*, 88(16):3248–3248, November 2018. ISSN 0094-9655, 1563-5163. doi: 10.1080/00949655.2018.1505197. URL <https://www.tandfonline.com/doi/full/10.1080/00949655.2018.1505197>.

- Patrik Reizinger, Yash Sharma, Matthias Bethge, Bernhard Schölkopf, Ferenc Huszár, and Wieland Brendel. Jacobian-based Causal Discovery with Nonlinear ICA. *Transactions on Machine Learning Research*, 2023, April 2023. ISSN 2835-8856. URL <https://openreview.net/forum?id=2Yo9xqR6Ab>.
- Patrik Reizinger, Alice Bizeul, Attila Juhos, Julia E. Vogt, Randall Balestriero, Wieland Brendel, and David Klindt. Cross-Entropy Is All You Need To Invert the Data Generating Process. In *ICLR*, October 2024a. URL <https://openreview.net/forum?id=hrqN0xpItr>.
- Patrik Reizinger, Siyuan Guo, Ferenc Huszár, Bernhard Schölkopf, and Wieland Brendel. Identifiable Exchangeable Mechanisms for Causal Structure and Representation Learning. October 2024b. URL <https://openreview.net/forum?id=k03mB4lvym>.
- Peter M Robinson. Root-n-consistent semiparametric regression. *Econometrica: Journal of the Econometric Society*, 56(4):931–954, 1988. doi: 10.2307/1912705. URL <https://doi.org/10.2307/1912705>.
- Paul Rolland, Volkan Cevher, Matthäus Kleindessner, Chris Russell, Dominik Janzing, Bernhard Schölkopf, and Francesco Locatello. Score Matching Enables Causal Discovery of Nonlinear Additive Noise Models. In *Proceedings of the 39th International Conference on Machine Learning*, pages 18741–18753. PMLR, June 2022. URL <https://proceedings.mlr.press/v162/rolland22a.html>. ISSN: 2640-3498.
- Paul R Rosenbaum and Donald B Rubin. The central role of the propensity score in observational studies for causal effects. *Biometrika*, 70(1):41–55, 1983. doi: 10.21236/ada114514. URL <https://doi.org/10.21236/ada114514>.
- Megan S. Schuler and Sherri Rose. Targeted Maximum Likelihood Estimation for Causal Inference in Observational Studies. *American Journal of Epidemiology*, 185(1):65–73, January 2017. ISSN 0002-9262. doi: 10.1093/aje/kww165. URL <https://doi.org/10.1093/aje/kww165>.
- Shohei Shimizu, Patrik O Hoyer, Aapo Hyvarinen, and Antti Kerminen. A Linear Non-Gaussian Acyclic Model for Causal Discovery. *J. Mach. Learn. Res.*, 7: 28, 2006. URL <https://jmlr.org/papers/v7/shimizu06a.html>.
- Shohei Shimizu, Takanori Inazumi, Yasuhiro Sogawa, Aapo Hyvärinen, Yoshinobu Kawahara, Takashi Washio, Patrik O. Hoyer, and Kenneth Bollen. DirectLiNGAM: A direct method for learning a linear non-Gaussian structural equation model. *Journal of Machine Learning Research*, 12:1225–1248, 2011. URL <https://jmlr.org/papers/v12/shimizulla.html>.
- Peter Spirtes and Kun Zhang. Causal discovery and inference: concepts and recent methodological advances. *Applied Informatics*, 3(1):3, February 2016. ISSN 2196-0089. doi: 10.1186/s40535-016-0018-x. URL <https://doi.org/10.1186/s40535-016-0018-x>.
- Daniele Tramontano, Yaroslav Kivva, Saber Salehkaleybar, Mathias Drton, and Negar Kiyavash. Causal Effect Identification in LiNGAM Models with Latent Confounders, June 2024. URL <http://arxiv.org/abs/2406.02049>. arXiv:2406.02049 [cs, stat].
- Liang Wendong, Armin Kekić, Julius von Kügelgen, Simon Buchholz, Michel Besserve, Luigi Gresele, and Bernhard Schölkopf. Causal Component Analysis, October 2023. URL <http://arxiv.org/abs/2305.17225>. arXiv:2305.17225 [cs, stat].
- Qingyan Xiang, Yubai Yuan, Dongyuan Song, Usman J Wudil, Mukhtar H Aliyu, C William Wester, and Bryan E Shepherd. Double machine learning to estimate the effects of multiple treatments and their interactions. *arXiv preprint arXiv:2505.12617*, 2025.
- Dehan Kong Xiaochuan Shi and Linbo Wang. Simultaneous estimation of multiple treatment effects from observational studies. *Journal of Computational and Graphical Statistics*, 0(ja):1–16, 2025. doi: 10.1080/10618600.2024.2449074. URL <https://doi.org/10.1080/10618600.2024.2449074>.
- Ying Zhu, Zhuqing Yu, and Guang Cheng. High Dimensional Inference in Partially Linear Models. In *Proceedings of the Twenty-Second International Conference on Artificial Intelligence and Statistics*, pages 2760–2769. PMLR, April 2019. doi: 10.2139/ssrn.3015397. URL <https://proceedings.mlr.press/v89/zhu19c.html>. ISSN: 2640-3498.

Estimating Treatment Effects with Independent Component Analysis (Supplementary Material)

Patrik Reizinger^{†1,2}

Lester Mackey³

Wieland Brendel¹

Rahul G. Krishnan^{2,4}

¹Max Planck Institute for Intelligent Systems & ELLIS Institute, Tübingen, Germany

²Vector Institute, Toronto, Canada

³Microsoft Research, New England, USA

⁴Department of Computer Science, University of Toronto, Toronto, Canada

CONTENTS

A	Insights from Score-Based Causal Discovery	15
B	Moment Conditions in Higher-Order OML and ICA	16
B.1	Higher-order OML moment condition for whitened data and $r = 3$	16
B.2	ICA moment condition for whitened data and kurtosis loss	16
C	Proofs	17
C.1	Proof of Lemma 3.1	17
C.2	Proof of Corollary 3.2	17
C.3	Proof of Theorem 3.1: Asymptotic relative efficiency	17
C.4	Proof of Corollary 3.3	21
D	Compute Usage	22
E	Additional Experiments: Treatment Noise and PLR Coefficient Ablations	22
E.1	Demand Estimation Ablations	22
E.2	Treatment Noise Distribution Ablation Study	22
E.3	Treatment Noise Variance Ablation Study	23
E.4	Coefficient Ablation Study	24
E.5	Summary	28
E.6	Nonlinear PLR Ablations	28
E.7	Multiple Treatment Ablations	30

*This work was initiated during P.R.'s internship at the Vector Institute. Correspondence to: patrik.reizinger@tuebingen.mpg.de

†This work was initiated during P.R.'s internship at the Vector Institute. Correspondence to: patrik.reizinger@tuebingen.mpg.de

E.8 FastICA Ablations	30
E.9 FastICA vs. DirectLiNGAM Comparison	30
E.10 Summary	33

Algorithm 1: FastICA (deflationary) with generic non-Gaussianity measure U . [Hyvarinen et al., 2001]

Inputs: $\mathbf{X} \in \mathbb{R}^{d \times n}$ (columns are observed samples), target components $m \leq d$, tolerance $\varepsilon > 0$, maximum iterations T_{\max}

Outputs: $\mathbf{W} \in \mathbb{R}^{m \times d}$ (unmixing matrix), $\mathbf{S} = \mathbf{W} \tilde{\mathbf{X}} \in \mathbb{R}^{m \times n}$ (independent components)

Centering:

$\bar{\mathbf{x}} \leftarrow \frac{1}{n} \mathbf{X} \mathbf{1}$; $\mathbf{X} \leftarrow \mathbf{X} - \bar{\mathbf{x}} \mathbf{1}^\top$ // Zero-mean the data

Whitening:

$\mathbf{C} \leftarrow \frac{1}{n} \mathbf{X} \mathbf{X}^\top$; $\mathbf{C} = \mathbf{O} \mathbf{D} \mathbf{O}^\top$ // Eigenvalue decomposition of covariance

$\mathbf{V} \leftarrow \mathbf{D}^{-1/2} \mathbf{O}^\top$; $\tilde{\mathbf{X}} \leftarrow \mathbf{V} \mathbf{X}$ // Whitened data

Initialize

$\mathbf{W} \leftarrow \mathbf{0}_{m \times d}$

for $i \leftarrow 1$ **to** m **do**

 Choose random $\mathbf{w} \in \mathbb{R}^d$;

$\mathbf{w} \leftarrow \mathbf{w} / \|\mathbf{w}\|_2$ // Unit-norm initialization

for $t \leftarrow 1$ **to** T_{\max} **do**

$\mathbf{o} \leftarrow \mathbf{w}^\top \tilde{\mathbf{X}}$ // $1 \times n$ projected samples

 // Fixed-point (Newton) update

$\mathbf{w}^+ \leftarrow \frac{1}{n} \tilde{\mathbf{X}} U'(\mathbf{o})^\top - \left(\frac{1}{n} \sum_{j=1}^n U''(u_j) \right) \mathbf{w}$

 // Deflationary orthogonalization (Gram-Schmidt) w.r.t. previous components

for $k \leftarrow 1$ **to** $i - 1$ **do**

$\mathbf{w}^+ \leftarrow \mathbf{w}^+ - (\mathbf{w}^{+\top} \mathbf{w}_k) \mathbf{w}_k$

end

$\mathbf{w}^+ \leftarrow \mathbf{w}^+ / \|\mathbf{w}^+\|_2$ // Normalization

if $|\mathbf{w}^{+\top} \mathbf{w} - 1| < \varepsilon$ **then**

break

end

$\mathbf{w} \leftarrow \mathbf{w}^+$

end

$\mathbf{w}_i \leftarrow \mathbf{w}^+$; $\mathbf{W}_{i,:} \leftarrow \mathbf{w}_i^\top$ // Store component i

end

Recover sources:

$\mathbf{S} \leftarrow \mathbf{W} \tilde{\mathbf{X}}$ // Independent components

A INSIGHTS FROM SCORE-BASED CAUSAL DISCOVERY

Recent works [Rolland et al., 2022, Montagna et al., 2023b, 2024, 2023a] utilized the (Jacobian of) the score function (the derivative of the log-likelihood) for causal discovery. Treatment effect estimation can be thought of as generalizing CD: the treatment effect informs us about the “strength” of a causal effect, whereas CD only seeks to determine the presence or absence of the edges. We will use this connection to show that if the goal is to solve a partial BSS problem by recovering only some of the sources then the non-Gaussianity condition can be relaxed on the covariates. To this end, consider the log likelihood of the PLR model (1) when ε and η are Gaussian (we only use Gaussians for illustration purposes):

$$\log p(Z) = -\frac{1}{2}(Y - f(X) - \theta T)^2 - \frac{1}{2}(T - g(X))^2 + \log p(X). \quad (8)$$

Irrespective of the distribution of X , we can differentiate with respect to T and Y to isolate the causal effect:

$$\partial_T \log p(Z) = g(X) - T + \theta(Y - f(X) - \theta T) \quad (9)$$

$$= -\eta + \theta \varepsilon; \quad (10)$$

$$\partial_{T,Y}^2 \log p(Z) = \theta. \quad (11)$$

The intuitive takeaway from the above is that due to the additive structure of the treatment effect, taking derivatives help

B MOMENT CONDITIONS IN HIGHER-ORDER OML AND ICA

B.1 HIGHER-ORDER OML MOMENT CONDITION FOR WHITENED DATA AND $r = 3$

To achieve \sqrt{n} -consistency with higher-order robustness to nuisance errors, the higher-order OML estimator of Mackey et al. [2018, Thm. 9] requires the following moment condition on the treatment noise η that rules out the Gaussian distribution: for some $r \geq 2, r \in \mathbb{N}$,

$$\mathbb{E} [\eta^{r+1}] \neq r \mathbb{E} [\mathbb{E} [\eta^2 | X] \cdot \mathbb{E} [\eta^{r-1} | X]]. \quad (12)$$

The two sides in (12) are equal for when $\eta | X$ is Gaussian. When η has unit variance and $r = 3$, this condition is equivalent to non-zero excess kurtosis.

Lemma B.1 (Higher-order OML moment condition for whitened data and $r = 3$). *When the treatment noise is assumed to have zero mean and unit variance, and $r = 3$, then (12) is equal to $\mathbb{E}(\eta^4) \neq 3$, i.e., it measures the kurtosis of η and rules out a Gaussian.*

Proof. The Higher-order Orthogonal Machine Learning (HOML) estimator uses a test function $U'(\eta) = \eta^r$ for estimating θ . Furthermore, we have the condition that excludes the Gaussian (for $r = 3$):¹

$$\mathbb{E} [\eta^{r+1}] \neq r \mathbb{E} [\mathbb{E} [\eta^2 | X] \cdot \mathbb{E} [\eta^{r-1} | X]]. \quad (13)$$

By assuming $\eta \perp X$,

$$= r \mathbb{E} [\mathbb{E} [\eta^2] \cdot \mathbb{E} [\eta^{r-1}]]. \quad (14)$$

With the unit variance constraint on η , we get

$$= r \mathbb{E} [\eta^{r-1}], \quad (15)$$

which, for $r = 3$ yields

$$\mathbb{E} [\eta^4] \neq 3 \mathbb{E} [\eta^2]. \quad (16)$$

Noting that the RHS is the variance, we can simplify by the whitening assumption:

$$\mathbb{E} [\eta^4] \neq 3, \quad (17)$$

i.e., η cannot not be a standard normal RV Since we assumed $\eta \perp X$ and that $\mathbb{E}\eta^2 = 1$ (unit variance, which is implied by the whitening preprocessing in ICA). \square

B.2 ICA MOMENT CONDITION FOR WHITENED DATA AND KURTOSIS LOSS

ICA has a similar condition to higher-order OML (cf. § B.1) for the local optima under the constraint that $\|\mathbf{w}\| = 1$, which ensures that the FastICA gradient is non-zero [Hyvarinen et al., 2001, A.8]:

$$\mathbb{E} [\eta \cdot U'(\eta) - U''(\eta)] \neq 0, \quad (18)$$

where t is a test function and the data is assumed to be whitened (proof in § B.2).

Lemma B.2 (ICA moment condition for whitened data and kurtosis loss). *Assume a linear ICA model with $\mathbb{E}[U(\eta)] = \mathbb{E}[\eta^4]$ as a loss function, whitened data, and constrain the rows of the unmixing matrix such that $\|\mathbf{w}\| = 1$. Then (18) is equivalent to $\mathbb{E}(\eta^4) \neq 3$.*

¹This is required to fulfil the non-degeneracy condition, i.e., to avoid that the expectation of $\nabla_{\theta} m$ is 0

Proof. To see the connection to ICA, we recall [Hyvärinen and Oja, 2000, Thm. 8.1], stating that for the estimated sources, i.e., the local optima of $\mathbb{E}_{U(\hat{\eta})}$, where U is generally chosen as $U(\eta) = \eta^4$, the optimality condition of the theorem is:

$$\mathbb{E} [\eta \cdot U'(\eta) - U''(\eta)] \neq 0, \quad (19)$$

which becomes for the kurtosis-based formulation (i.e., when $U(\eta) = \eta^4$):

$$\mathbb{E} [\eta^4 - 3\eta^2] \neq 0. \quad (20)$$

Or, equivalently:

$$\mathbb{E} [\eta^4] \neq \mathbb{E} [3\eta^2] = 3. \quad (21)$$

□

C PROOFS

C.1 PROOF OF LEMMA 3.1

Proposition 3.1 (Treatment effect estimation with ICA). *When Assum. 3.1 holds and $\text{Var}(\varepsilon) = 1$, linear ICA identifies the causal effect θ at the global optimum of the loss in the infinite sample limit.*

Proof. We can apply the theory of linear ICA [Shimizu et al., 2006, Hyvärinen and Oja, 2000] to identify the sources (in the infinite data limit) up to scaling and permutation. Then, exploiting that \mathbf{A} is triangular, we can permute its estimated inverse $\mathbf{W} = \mathbf{A}^{-1}$ into a lower triangular form. Thus, by knowing the graph (particularly that Y is a leaf node), we can resolve the permutation indeterminacy. Thus, we have the estimate of ε and the corresponding row in \mathbf{W} . ICA is invariant to scaling the rows of \mathbf{W} ; however, assuming a specific form of how ε affects Y is sufficient to resolve this ambiguity. Finally, selecting the entry characterizing the $T \rightarrow \varepsilon$ relationship gives us the causal effect θ . □

C.2 PROOF OF COROLLARY 3.2

Proposition 3.2 (Estimating multiple treatment effects with ICA). *Under Assum. 3.1 in the multiple treatment linear PLR model (Defn. 3.2), ICA identifies all treatment effects at the global optimum of the loss in the infinite sample limit.*

Proof. We can apply the theory of linear ICA [Shimizu et al., 2006, Hyvärinen and Oja, 2000] to identify the sources (in the infinite data limit) up to scaling and permutation. Then, exploiting that \mathbf{A} is triangular and that Y is a leaf node, we can permute its estimated inverse $\mathbf{W} = \mathbf{A}^{-1}$ into a lower triangular form. However, as opposed to Prop. 3.1, this does not resolve the permutation between the different treatment variables, as permuting (η_1, η_2) keeps \mathbf{W} triangular. However, the knowledge of the graph (which variable is which treatment component) enables us to resolve this ambiguity. Thus, we have the estimate of ε and the corresponding row in \mathbf{W} . ICA is invariant to scaling the rows of \mathbf{W} ; however, assuming a specific form (a PLR model with unit variance ε) of how ε affects Y is sufficient to resolve this ambiguity.

Finally, selecting the entries characterizing the $T_1, T_2 \rightarrow \varepsilon$ relationship gives us the causal effects θ_1, θ_2 . □

C.3 PROOF OF THEOREM 3.1: ASYMPTOTIC RELATIVE EFFICIENCY

We compare the asymptotic variances of both higher-order OML [Mackey et al., 2018] and FastICA [Hyvärinen and Oja, 1997] estimators. We are able to do this as the asymptotic normality of the treatment effect estimate is implied by the stated assumptions. In the following, we will denote the asymptotic variance of the estimated parameter $\hat{\theta}$ as:

$$\text{AsymptoticVariance}(\hat{\theta}) \triangleq \lim_{n \rightarrow \infty} \text{Var}(\sqrt{n}(\hat{\theta} - \theta)). \quad (22)$$

C.3.1 Assumptions

We include all assumptions of both Thm. 4.5 of [Auddy and Yuan \[2023\]](#) and those of Thm. 9 of [Mackey et al. \[2018\]](#) that are required for our asymptotic variance results.

Assumption C.1 (Auddy–Yuan ICA distribution class and CLT regime). Let $Z \in \mathbb{R}^d$ denote the observed vector to which we apply ICA. (In our PLR application, $d = p + 2$ and $Z = (X^\top, T, Y)^\top$.) Let \tilde{Z} be a whitened version of Z , e.g.

$$\tilde{Z} \triangleq \text{Cov}(Z)^{-1/2} Z, \quad \text{so that} \quad \text{Cov}(\tilde{Z}) = I_d.$$

Assume \tilde{Z} follows a (whitened) ICA model

$$\tilde{Z} = AS, \quad A \in \mathcal{O}(d),$$

where $S = (S_1, \dots, S_d)^\top$ has mutually independent coordinates.

(Source normalization.) For every $j \in [d]$, $\mathbb{E}[S_j] = 0$ and $\mathbb{E}[S_j^2] = 1$.

(Non-Gaussianity and moment bounds.) There exist constants $\epsilon_1 > 0$ and $M_1, M_2 > 0$ such that for every $j \in [d]$,

$$M_1^{-1} \leq |\kappa_4(S_j)| \leq M_1, \quad \mathbb{E}[|S_j|^{8+\epsilon_1}] \leq M_2,$$

where $\kappa_4(S_j) \triangleq \mathbb{E}[S_j^4] - 3$ is the excess kurtosis.

(Auddy–Yuan Thm. 4.5 additional requirements.) For the bilinear-form normal approximation in [Auddy and Yuan \[2023\]](#), Thm. 4.5], assume further:

1. $\epsilon_1 \geq 4$ (so the sources have at least $(8 + 4) = 12$ finite moments);
2. the sample $\tilde{Z}_1, \dots, \tilde{Z}_n$ consists of i.i.d. copies of \tilde{Z} ;
3. the high-dimensional sample size regime $n \geq Cd^3(\log d)^2$ holds for a sufficiently large universal constant $C > 0$;
4. for the specific vectors $u, v \in \mathbb{R}^d$ defining the bilinear functional $u^\top(\hat{A} - A)v$, the asymptotic variance $\sigma_{u,v}^2$ from [Auddy and Yuan \[2023\]](#), Thm. 4.5] is non-degenerate:

$$\liminf_{d \rightarrow \infty} \sigma_{u,v} > 0.$$

Equivalently, in the notation of [Auddy and Yuan \[2023\]](#), Thm. 4.5], the law of \tilde{Z} belongs to the ICA class

$$\mathcal{P}_{\text{ICA}}(A; \epsilon_1, M_1, M_2) \triangleq \left\{ \mathcal{L}(\tilde{Z}) : \tilde{Z} = AS, A \in \mathcal{O}(d), (S_j)_{j=1}^d \text{ indep.}, \right. \\ \left. \mathbb{E}[S_j] = 0, \mathbb{E}[S_j^2] = 1, M_1^{-1} \leq |\kappa_4(S_j)| \leq M_1, \mathbb{E}[|S_j|^{8+\epsilon_1}] \leq M_2 \right\}.$$

Remark C.1 (Meaning of Assumption C.1). Assumption C.1 packages two layers of conditions:

1. **Whitening / orthogonal mixing** ($A \in \mathcal{O}(d)$). Whitening enforces $\text{Cov}(\tilde{Z}) = I_d$, which reduces the general ICA ambiguity to an *orthogonal* mixing matrix A . This is analytically convenient because the unmixing matrix is $A^{-1} = A^\top$.
2. **Source normalization** ($\mathbb{E}[S_j] = 0, \mathbb{E}[S_j^2] = 1$). ICA is invariant to componentwise rescaling: replacing S_j by $c_j S_j$ can be absorbed by rescaling the corresponding column of A . The mean/variance constraints fix this scale indeterminacy (up to sign).
3. **Uniform non-Gaussianity via kurtosis bounds**. The lower bound $|\kappa_4(S_j)| \geq M_1^{-1}$ prevents components from being (nearly) Gaussian, which would make kurtosis-based identification ill-conditioned. The upper bound $|\kappa_4(S_j)| \leq M_1$ prevents extremely heavy-tailed sources from dominating fourth-order statistics.
4. **High-moment control** ($\mathbb{E}[|S_j|^{8+\epsilon_1}] \leq M_2$). This ensures that empirical higher-order statistics (used by kurtosis-based ICA procedures) concentrate around their population values. In [Auddy and Yuan \[2023\]](#), Thm. 4.5] they require the stronger $\epsilon_1 \geq 4$ so that $(8 + \epsilon_1) \geq 12$ moments exist, which is used to obtain a Berry–Esseen-type normal approximation for bilinear forms of the ICA estimator.

5. **High-dimensional CLT scaling** ($n \gtrsim d^3(\log d)^2$). Theorem 4.5 is a *high-dimensional* normal approximation bound. The scaling $n \geq Cd^3(\log d)^2$ is a sufficient regime ensuring the non-asymptotic remainder terms in the normal approximation are $o(1)$ as $d \rightarrow \infty$.
6. **Non-degenerate variance** ($\liminf \sigma_{u,v} > 0$). The bilinear functional $u^\top(\widehat{A} - A)v$ can be asymptotically degenerate for particular choices of (u, v) (e.g. if the leading variance term cancels). The condition $\sigma_{u,v}$ bounded away from 0 ensures the limiting Gaussian has positive variance, so a meaningful CLT statement applies.

Assumption C.2 (Assumptions of Thm. 4.5 of [Auddy and Yuan \[2023\]](#)). (i) Let $X \in \mathbb{R}^d$ follow a (whitened) ICA model $X = AS$, $A \in \mathcal{O}(d)$, where $S = (S_1, \dots, S_d)^\top$ has independent components.
(ii) Assume there exist constants $\epsilon \geq 4$ and $M_1, M_2 > 0$ such that for all $j \in [d]$,

$$\mathbb{E}[S_j] = 0, \quad \mathbb{E}[S_j^2] = 1, \quad (23)$$

$$M_1^{-1} \leq |\kappa_4(S_j)| \leq M_1, \quad \mathbb{E}|S_j|^{8+\epsilon} \leq M_2, \quad (24)$$

where $\kappa_4(S_j) := \mathbb{E}[S_j^4] - 3$ denotes the excess kurtosis.

- (iii) Let X_1, \dots, X_n be i.i.d. copies of X .
(iv) For the bilinear-form CLT in [Auddy and Yuan \[2023, Thm. 4.5\]](#), additionally assume: (i) $n \geq Cd^3(\log d)^2$ for a universal constant $C > 0$, and (ii) for the specific $u, v \in \mathbb{R}^d$ of interest, the asymptotic variance is nondegenerate,

$$\liminf_{d \rightarrow \infty} \sigma_{u,v} > 0,$$

where $\sigma_{u,v}^2 := u^\top AD_v A^\top u$ (with D_v as defined in [Auddy and Yuan \[2023, Thm. 4.5\]](#)).

Assumption C.3 (Assumptions of Thm. 9 of [Mackey et al. \[2018\]](#)). (i) (PLR model) Observe $Z = (T, Y, X)$ satisfying

$$\begin{aligned} Y &= \theta_0 T + f_0(X) + \varepsilon, & \mathbb{E}[\varepsilon \mid X, T] &= 0 \text{ a.s.}, \\ T &= g_0(X) + \eta, & \mathbb{E}[\eta \mid X] &= 0 \text{ a.s.}, \end{aligned}$$

where (η, ε) are unobserved disturbances with distributions independent of (θ_0, f_0, g_0) .

- (ii) (Non-Gaussian treatment residual) Assume there exists $r \in \mathbb{N}$ such that

$$\mathbb{E}[\eta^{r+1}] \neq r \mathbb{E}[\mathbb{E}[\eta^2 \mid X] \mathbb{E}[\eta^{r-1} \mid X]].$$

Equivalently (as used by [Mackey et al. \[2018, Thm. 9\]](#)), the conditional distribution of $\eta \mid X$ is not almost surely Gaussian.

- (iii) Define the second-order orthogonality multi-index set

$$\mathcal{S} := \{\alpha \in \mathbb{N}^4 : \|\alpha\|_1 \leq 2\} \setminus \{(1, 0, 0, 1), (0, 1, 0, 1)\}.$$

Multi-index notation and the meaning of the second-order orthogonality set. In [Mackey et al. \[2018, Thm. 9\]](#), the moment function depends on a vector of *four* nuisance functions

$$h(x) \equiv (h_1(x), h_2(x), h_3(x), h_4(x)) := (q(x), g(x), \mu_{r-1}(x), \mu_r(x)),$$

where typically $\mu_k(x) := \mathbb{E}[\eta^k \mid X = x]$ and q, g are nuisance regressions.

For a multi-index $\alpha = (\alpha_1, \alpha_2, \alpha_3, \alpha_4) \in \mathbb{N}^4$, define its total order $|\alpha|_1 := \sum_{j=1}^4 \alpha_j$. Let $D^\alpha m$ denote the mixed partial derivative of m with respect to the *nuisance coordinates*:

$$D^\alpha m(z; \theta; h) := \frac{\partial^{|\alpha|_1}}{\partial h_1^{\alpha_1} \partial h_2^{\alpha_2} \partial h_3^{\alpha_3} \partial h_4^{\alpha_4}} m(z; \theta; h),$$

evaluated at $h = h_0(X)$ (i.e., at the true nuisance values).

S-orthogonality. Given a set $\mathcal{S} \subseteq \mathbb{N}^4$, the moment m is called \mathcal{S} -orthogonal (w.r.t. h_0) if

$$\mathbb{E}[D^\alpha m(Z; \theta_0; h_0(X)) \mid X] = 0, \quad \forall \alpha \in \mathcal{S}.$$

The “second-order orthogonality multi-index set” used in **Thm. 9**. Mackey et al. use the set

$$\mathcal{S} := \left\{ \alpha \in \mathbb{N}^4 : |\alpha|_1 \leq 2 \right\} \setminus \{(1, 0, 0, 1), (0, 1, 0, 1)\}.$$

This means: *all* conditional expectations of mixed nuisance-derivatives of total order ≤ 2 are required to vanish, *except* the two cross-derivatives that couple the fourth nuisance coordinate $h_4 = \mu_r$ with $h_1 = q$ or $h_2 = g$.

Equivalently, \mathcal{S} -orthogonality with the above \mathcal{S} is the collection of conditions

$$\begin{aligned} \mathbb{E} \left[\frac{\partial m}{\partial h_j}(Z; \theta_0; h_0(X)) \middle| X \right] &= 0, & j = 1, 2, 3, 4, \\ \mathbb{E} \left[\frac{\partial^2 m}{\partial h_j^2}(Z; \theta_0; h_0(X)) \middle| X \right] &= 0, & j = 1, 2, 3, 4, \\ \mathbb{E} \left[\frac{\partial^2 m}{\partial h_j \partial h_k}(Z; \theta_0; h_0(X)) \middle| X \right] &= 0, & 1 \leq j < k \leq 4, (j, k) \notin \{(1, 4), (2, 4)\}. \end{aligned}$$

In words: m is “second-order orthogonal” in every nuisance direction and every pairwise interaction *except* it does not enforce orthogonality for the mixed interactions (q, μ_r) and (g, μ_r) .

C.3.2 Asymptotic variance of higher-order OML

We state the asymptotic variance of the higher-order OML estimator from [Mackey et al., 2018, Thm. 9].

For **OML**, the asymptotic variance for θ is (with test function U)

$$\text{Var}(\theta_{\text{OML}}) = J^{-1} V J^{-1}, \quad (25)$$

$$J = \mathbb{E}[\nabla_{\theta} m] \quad \text{and} \quad V = \text{Cov}(m), \quad (26)$$

$$\nabla_{\theta} m = \varepsilon(U'(\eta) - \mathbb{E}[U'(\eta)] - \eta \mathbb{E}[U''(\eta)]), \quad (27)$$

$$J = \mathbb{E}[\eta U'(\eta) - \eta^2 \mathbb{E}[U''(\eta)]]. \quad (28)$$

For unit variance, this simplifies to

$$J = \mathbb{E}[\eta U'(\eta) - U''(\eta)]. \quad (29)$$

yielding the asymptotic variance for the outcome noise $\varepsilon = Y - q(X) - \theta \eta$

$$\text{AsymptoticVariance}(\hat{\theta}_{\text{OML}}) = \frac{\mathbb{E}[\varepsilon^2(U'(\eta) - \mathbb{E}[U'(\eta)] - \eta \mathbb{E}[U''(\eta)])^2]}{(\mathbb{E}[\eta U'(\eta) - \eta^2 \mathbb{E}[U''(\eta)]])^2}. \quad (30)$$

As we assumed unit variance for the noises, this yields:

$$= \frac{\mathbb{E}[(U'(\eta) - \mathbb{E}[U'(\eta)] - \eta \mathbb{E}[U''(\eta)])^2]}{(\mathbb{E}[\eta U'(\eta) - \mathbb{E}[U''(\eta)]])^2}. \quad (31)$$

C.3.3 Asymptotic variance for FastICA

Setup. We consider the ICA model in the context of a partially linear regression (PLR) setup. Let $Z = \mathbf{B}S$, where $Z \in \mathbb{R}^d$ are the observed signals, S are the independent sources, and $\mathbf{B} \in \mathbb{R}^{d \times d}$ is the unwhitened mixing matrix. The whitened observations are $X = \Sigma^{-1/2}Z$, where $\Sigma = \text{Cov}(Z)$. Then the whitened mixing matrix is $\mathbf{A} = \Sigma^{-1/2}\mathbf{B}$, so $X = \mathbf{A}S$.

We want to compute the asymptotic variance of the FastICA estimate of $B_{3,2} = \theta$, the treatment effect in a PLR model.

Using [Auddy and Yuan, 2023, Thm 4.5]. Consider the vectors

$$u = \Sigma^{1/2} e_3, \quad v = e_2 \in \mathbb{R}^d, \quad (32)$$

which ensure that

$$u^\top (\widehat{\mathbf{A}} - \mathbf{A})v = e_3^\top (\widehat{\mathbf{B}} - \mathbf{B})e_2 = \widehat{B}_{3,2} - B_{3,2} = \widehat{\theta}_{ICA} - \theta. \quad (33)$$

Auddy and Yuan [2023, Thm 4.5] gives the asymptotic variance of the bilinear form $u^\top (\widehat{\mathbf{A}} - \mathbf{A})v$:

$$\sqrt{n} \cdot u^\top (\widehat{\mathbf{A}} - \mathbf{A})v \xrightarrow{d} \mathcal{N}(0, \sigma_{u,v}^2) \quad \text{with} \quad \sigma_{u,v}^2 = u^\top \mathbf{A} \mathbf{D}_v \mathbf{A}^\top u, \quad (34)$$

where \mathbf{D}_v is a diagonal matrix with diagonal entries

$$(D_v)_{kk} = \begin{cases} \frac{\text{Var}(S_2^3)}{\kappa_4(S_2)^2} & \text{if } k \neq 2, \\ 0 & \text{if } k = 2. \end{cases} \quad (35)$$

With this choice of u and v , the asymptotic variance is

$$\sigma_{u,v}^2 = u^\top \mathbf{A} \mathbf{D}_v \mathbf{A}^\top u = e_3^\top \mathbf{B} \mathbf{D}_v \mathbf{B}^\top e_3 = \sum_{k=1}^d B_{3k}^2 (D_v)_{kk}. \quad (36)$$

Thus,

$$\sigma_{u,v}^2 = \sum_{k \neq 2} B_{3k}^2 \cdot \frac{\text{Var}(S_2^3)}{\kappa_4(S_2)^2}, \quad (37)$$

where κ_4 is the excess kurtosis.

Substituting the PLR parameterization. In our partially linear regression model, the third row of \mathbf{B} is

$$B_{3,:} = (b + a\theta, \theta, 1). \quad (38)$$

So we obtain by plugging in $S_2 = \eta$:

$$\text{AsymptoticVariance}(\widehat{\theta}_{ICA}) = \sigma_{u,v}^2 = ((b + a\theta)^2 + 1) \cdot \frac{\text{Var}(\eta^3)}{\kappa_4(\eta)^2} = ((b + a\theta)^2 + 1) \cdot \frac{\text{Var}(U'(\eta))}{\mathbb{E}(\eta^4 - 3)^2}. \quad (39)$$

Remark C.2. If a, b are vectors, i.e., when X is vector-valued, then the above expression becomes:

$$\text{AsymptoticVariance}(\widehat{\theta}_{ICA}) = (\|b + a\theta\|_2^2 + 1) \cdot \frac{\text{Var}(\eta^3)}{\kappa_4(\eta)^2}. \quad (40)$$

C.4 PROOF OF COROLLARY 3.3

Proposition 3.3 (Treatment effect estimation with Gaussian covariates and ICA). *Consider the generalization of the linear PLR model (Defn. 3.1) with d covariates X . If $\text{Var}(\varepsilon) = 1$ and both ε and η are non-Gaussian, then linear ICA identifies the treatment effect at the global optimum of the loss in the infinite data limit (even if one or more covariates are Gaussian).*

Proof. The log-likelihood of observed causal variables is expressed with change-of-variables in terms of the noises:

$$\log p_Z(Z) = \log p_S(S) + \log |\det \mathbf{W}|,$$

where \mathbf{W} has the following structure

$$\mathbf{W} = \begin{bmatrix} \mathbf{I}_{\dim X} & 0 & 0 \\ \mathbf{A} & \mathbf{I}_{\dim T} & 0 \\ \mathbf{b} & \boldsymbol{\theta} & 1 \end{bmatrix}.$$

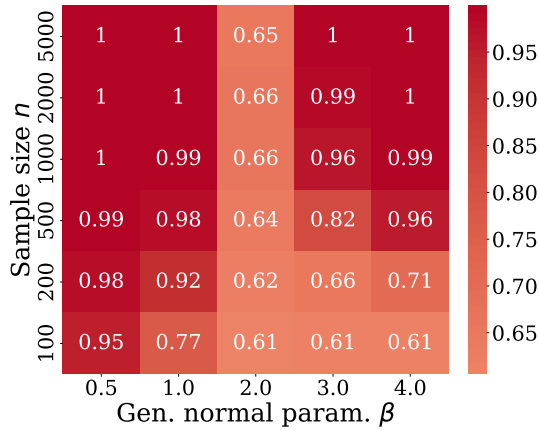


Figure E.1: **Source identification via Mean Correlation Coefficient (MCC) for ICA in linear PLR.** Means from 20 seeds ($d = 10$). MCC [Hyvarinen and Morioka, 2016] measures source recovery (0–1; higher is better). Gaussian covariates ($\beta = 2$) yield lowest MCC, as predicted by theory.

If the covariates have a Gaussian noise, then any rotation on the block of covariates will maintain the same likelihood—however, this will also change the direct effect coefficients of X on Y, T , i.e., $\mathbf{A} \in \mathbb{R}^{\dim T \times \dim X}$, $\mathbf{b} \in \mathbb{R}^{1 \times \dim X}$. Importantly, this does not change the treatment effect coefficients θ . That is, we can define an equivalence class $\mathbf{W}_O = \mathbf{W}\mathbf{O}$, where \mathbf{O} is a block-orthogonal matrix $\mathbf{O} = \text{diag}(\mathbf{O}_{\dim X}, \mathbf{I}_{\dim T}, 1)$ with $\mathbf{O}_{\dim X}$ being a $(\dim X \times \dim X)$ -dimensional orthogonal map. In this case, the inverse maps solving the BSS problem will capture the treatment effect. Thus, we can apply the same argument as in Prop. 3.1. Since both the treatment and outcome noise are non-Gaussian, they can be separated from the Gaussian covariate block by ICA. Thus, the treatment effect is identifiable. \square

D COMPUTE USAGE

All experiments ran on CPU-only nodes of an HTCondor cluster, each requesting 4 cores and 32 GB RAM. A single sweep of the full parameter grid comprises approximately 300 parallel jobs for the demand estimation experiments plus 10–20 ablation jobs, with individual runtimes ranging from under one hour (small sample sizes) to roughly two days ($n=5,000$). Including preliminary and debugging runs throughout the project, we estimate a total compute budget of approximately 50,000 CPU-hours. No GPUs were used.

E ADDITIONAL EXPERIMENTS: TREATMENT NOISE AND PLR COEFFICIENT ABLATIONS

This section provides supplementary experimental results that complement the main text, including additional ablation studies over ICA parameters, performance across different data generating processes, and extended comparisons with alternative methods.

E.1 DEMAND ESTIMATION ABLATIONS

These figures provide additional details for the demand estimation experiments in § 4.1. Fig. E.1 shows source identification quality measured by Mean Correlation Coefficient (MCC). Fig. E.2 shows MSE heatmaps across sample sizes and covariate dimensions or distribution shape parameters. Fig. E.3 shows RMSE and bias differences between ICA and higher-order OML for filtered configurations ($c_{\text{ICA}} < 1.5$; treatment coefficient $a = 0.5$, outcome coefficient $b = 0.05$, $\theta = 1$).

E.2 TREATMENT NOISE DISTRIBUTION ABLATION STUDY

We study how the treatment noise distribution η affects the relative performance of higher-order OML and ICA estimators.

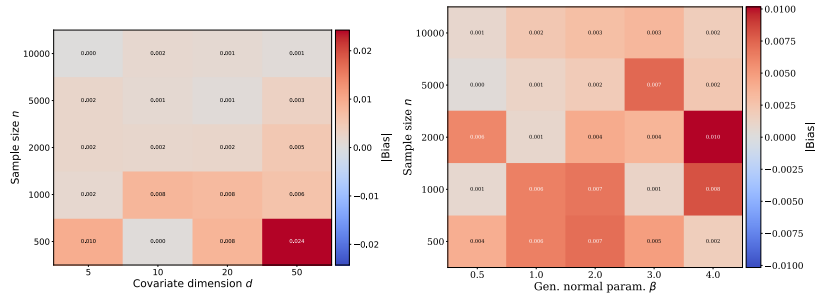


Figure E.2: **Treatment effect estimation MSE for ICA with multinomial treatment noise in linear PLR.** Means from 20 seeds; blue = lower, red = higher relative MSE. **Left:** Covariate dimension d vs. sample size ($\beta = 1$). **Right:** Generalized normal shape parameter β of the covariate noise density vs. sample size ($d = 10$).

E.2.1 Experimental Setup

All experiments use $n = 5,000$ samples, $d = 10$ covariates (support size), and 20 seeds per configuration. We employ 2-fold cross-fitting for nuisance function estimation. To ensure robustness, we randomize the model coefficients: $\theta \in [0.001, 5]$, $a \in [-10, 10]$, and $b \in [-0.5, 0.5]$, with 20 random configurations per noise distribution.

We evaluate four noise distributions for the treatment noise η spanning heavy-tailed and bounded regimes (κ denotes the excess kurtosis):

- **Discrete:** Asymmetric distribution with mass at $\{0, -0.5, -2, -4\}$ and probabilities $(0.65, 0.2, 0.1, 0.05)$; $\kappa \approx 4.97$
- **Laplace:** Heavy-tailed with scale $1/\sqrt{2}$ for unit variance; $\kappa = 3.0$
- **Uniform:** Bounded on $[-\sqrt{3}, \sqrt{3}]$; $\kappa \approx -1.2$
- **Rademacher:** Binary $\{-1, +1\}$ with equal probability; $\kappa = -2.0$

E.2.2 Results: Noise Distribution Ablation

Fig. E.5 provides a detailed heatmap visualization sorted by excess kurtosis. ICA consistently achieves lower RMSE across all tested distributions, with particularly strong performance for heavy-tailed distributions (high kurtosis).

E.3 TREATMENT NOISE VARIANCE ABLATION STUDY

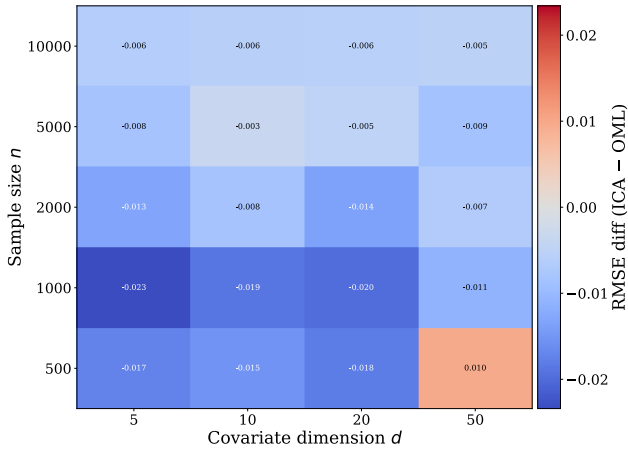
To further investigate the interplay between distribution shape and scale, we conduct a variance ablation study varying both the generalized normal shape parameter $\beta \in \{0.5, 1.0, 1.5, 2.5, 3.0, 4.0\}$ and variance $\sigma^2 \in \{0.25, 0.5, 1.0, 2.0, 4.0\}$. We exclude $\beta = 2$ (Gaussian) as ICA is not applicable when the noise is Gaussian. The treatment effect is fixed at $\theta = 1.0$ with $n = 5,000$ samples and 20 seeds.

E.3.1 Results: Variance Ablation

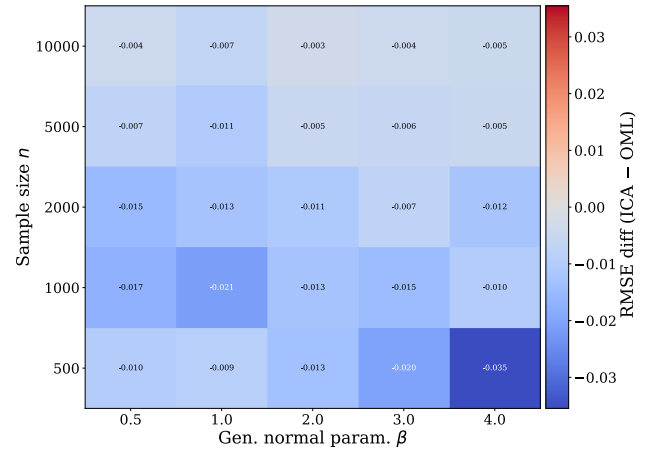
Figure E.4 presents the RMSE difference (ICA – higher-order OML) across the (β, σ^2) grid. Key findings include:

- For the heaviest-tailed distribution ($\beta = 0.5$), ICA outperforms higher-order OML across most variance levels, with the largest gains at low variance.
- For intermediate shape parameters ($\beta \in \{1.0, 1.5\}$), results are mixed: some configurations show large ICA advantages (e.g., $\beta = 1.0, \sigma^2 = 0.5$), but higher-order OML is competitive or better in other settings.
- For light-tailed distributions ($\beta \geq 2.5$), both methods perform similarly at moderate to high variance, while higher-order OML tends to be slightly better at low variance.

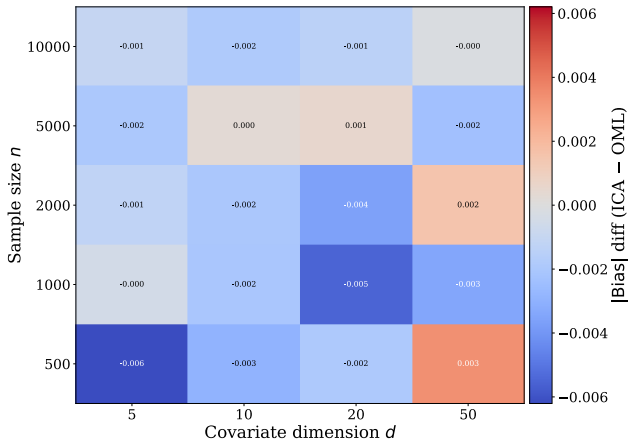
The excess kurtosis κ decreases monotonically with β : from $\kappa = 22.2$ at $\beta = 0.5$ to $\kappa = -0.81$ at $\beta = 4.0$. This confirms that ICA’s advantage is most pronounced when the treatment noise has high kurtosis (heavy tails), consistent with its theoretical asymptotic variance depending on κ^{-2} .



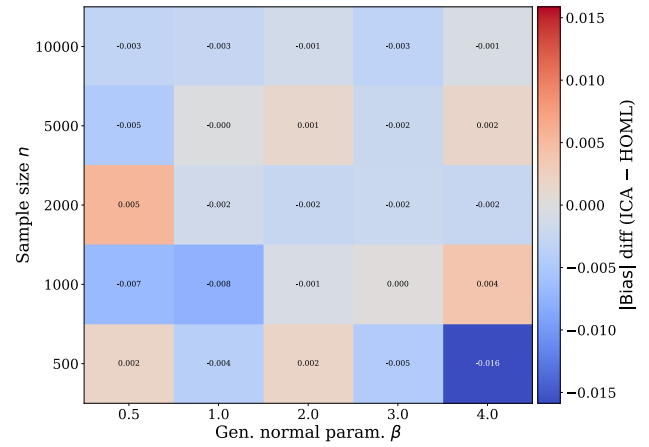
(a) RMSE difference vs. covariate dimension d



(b) RMSE difference vs. β



(c) Bias difference vs. covariate dimension d



(d) Bias difference vs. β

Figure E.3: **RMSE and bias differences (ICA – higher-order OML) in linear PLR.** Results filtered to configurations where $c_{ICA} < 1.5$. Coefficient vectors have a single non-zero entry: treatment coefficient $a = 0.5$, outcome coefficient $b = 0.05$, $\theta = 1$ (yielding $c_{ICA} = 1 + (b + a\theta)^2 \approx 1.30$). Means from 20 seeds; **blue** = ICA outperforms higher-order OML, **red** = higher-order OML outperforms ICA. **Top row:** RMSE differences. **Bottom row:** Bias differences. **Left column:** Covariate dimension d vs. sample size ($\beta = 4$). **Right column:** Generalized normal shape parameter β of the covariate noise density vs. sample size ($d = 10$).

E.4 COEFFICIENT ABLATION STUDY

We conduct systematic coefficient ablation experiments to understand how the structural parameters of the partially linear model affect the relative performance of higher-order OML and ICA estimators. Recall from [Thm. 3.1](#) that the ICA variance coefficient $c_{ICA} = 1 + \|b + a\theta\|_2^2$ directly scales ICA’s asymptotic variance.

E.4.1 Experimental Design

We systematically vary three coefficient parameters while holding the noise distribution fixed (discrete asymmetric distribution with $\kappa \approx 4.97$):

Coefficient Grid (Fixed). In the deterministic ablation, we use:

- Treatment coefficient: $a \in \{-0.002, 0.05, -0.43, 1.56\}$
- Outcome coefficient: $b \in \{0.003, -0.02, 0.63, -1.45\}$

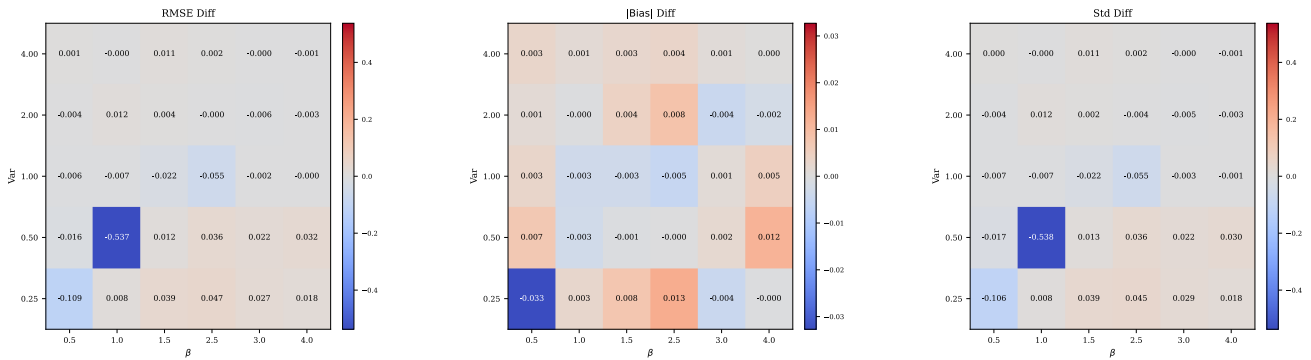


Figure E.4: **Estimation metric differences (ICA – higher-order OML) across the treatment noise variance ablation grid.** Panels show RMSE, absolute bias, and standard deviation differences (left to right). Rows correspond to generalized normal shape parameter β ; columns correspond to noise variance σ^2 . Blue cells indicate ICA outperforms higher-order OML; red cells indicate higher-order OML outperforms ICA.

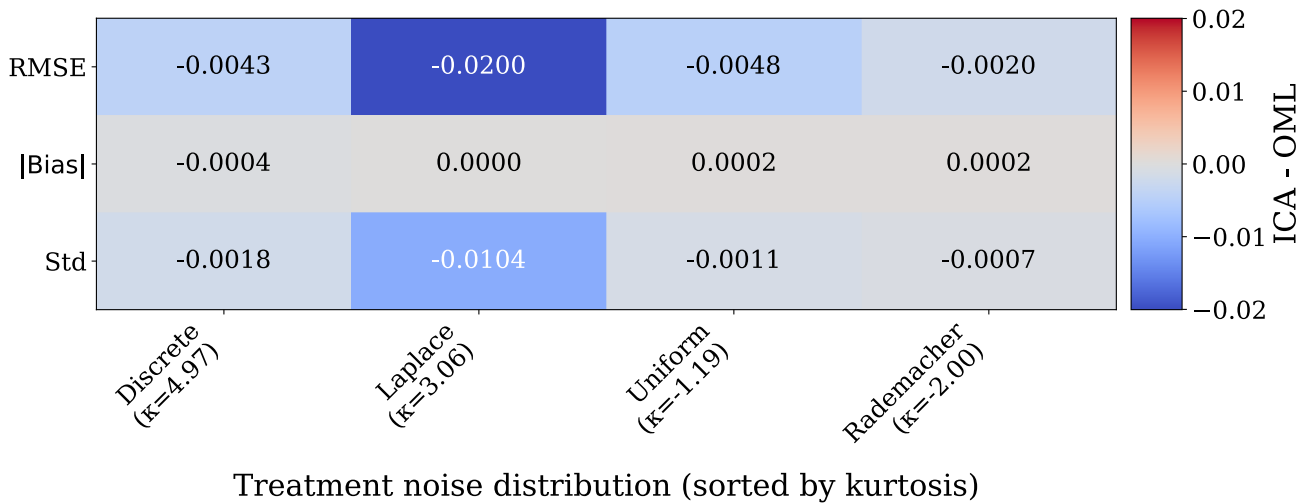


Figure E.5: **Heatmap of estimation performance differences (ICA – OML) across treatment noise distributions, sorted by excess kurtosis κ .** Blue cells indicate ICA outperforms OML; red cells indicate OML outperforms ICA.

- Treatment effect: $\theta \in \{0.01, 0.1, 0.5, 1.0, 3.0, 10.0\}$

This yields $4 \times 4 \times 6 = 96$ configurations. Only the first coefficient in each support is non-zero; remaining coefficients are set to zero.

Randomized Coefficients. We also conduct experiments with randomized coefficients—drawn from a uniform distribution—across multiple noise distributions:

- Treatment coefficient: $a \sim \mathcal{U}[-10, 10]$
- Outcome coefficient: $b \sim \mathcal{U}[-0.5, 0.5]$
- Treatment effect: $\theta \sim \mathcal{U}[0.001, 0.2]$

with 20 random configurations per noise distribution.

Common Settings. All experiments use $n = 5,000$ samples, $d = 10$ covariates, 20 seeds, 2-fold cross-fitting, and Lasso regularization (for OML) with $\lambda = \sqrt{\log(d)/n}$.

E.4.2 The Coefficient Cancellation Effect

A key finding is the *coefficient cancellation* phenomenon: when $b + a\theta \approx 0$, the ICA variance coefficient approaches its minimum value of 1, making ICA highly efficient. Table E.1 shows examples where near-perfect cancellation occurs.

Table E.1: Examples of coefficient cancellation where $c_{\text{ICA}} \approx 1$.

a	b	θ	c_{ICA}
-0.002	0.003	1.00	1.000001
0.050	-0.020	0.50	1.000025
-0.430	0.003	0.01	1.000002
0.050	-0.020	0.10	1.000049

Conversely, when coefficients reinforce rather than cancel, c_{ICA} can become very large. For instance, with $a = 1.56$, $b = 0.003$, and $\theta = 10$, we obtain $c_{\text{ICA}} = 244.45$.

E.4.3 Results: Performance Stratified by ICA Variance Coefficient

Figure E.6a shows how RMSE depends on the ICA variance coefficient. Fig. 2 right (in the main text, § 4) summarizes performance across different c_{ICA} regimes, showing that while ICA wins overall (72.9%), OML is preferable in the medium c_{ICA} regime.

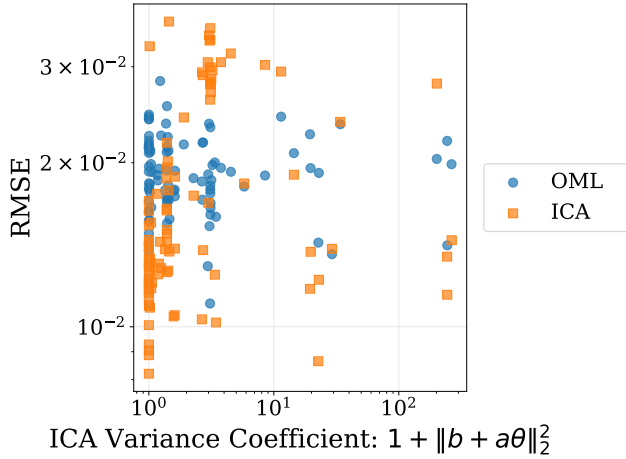
Key observations:

- **Low c_{ICA} regime:** ICA strongly dominates with 96.3% win rate, achieving 26% lower RMSE on average.
- **Medium c_{ICA} regime:** Higher-order OML becomes preferable, winning 64.3% of configurations.
- **High c_{ICA} regime:** Mixed results; ICA can still perform well despite high variance coefficient if other factors are favorable.

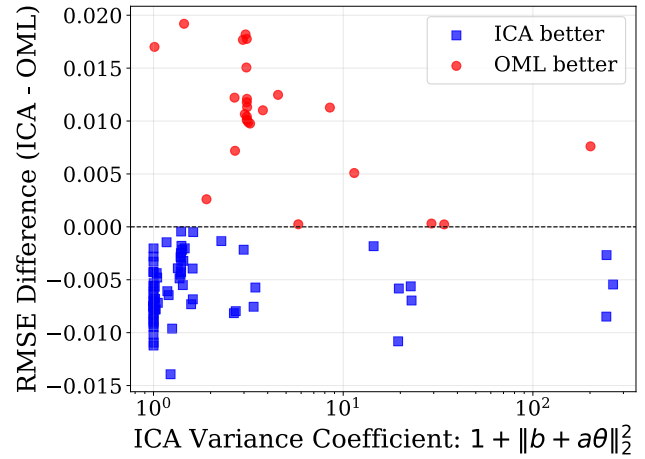
E.4.4 Results: Randomized Coefficients Across Distributions

Table E.2 shows results for randomized coefficient experiments across six noise distributions.

ICA consistently outperforms higher-order OML across all distributions when averaging over randomized coefficient configurations, with particularly strong advantages for heavy-tailed distributions (Laplace).



(a) RMSE vs. ICA variance coefficient $c_{\text{ICA}} = 1 + \|b + a\theta\|_2^2$ on log-log scale. Blue circles: higher-order OML; orange squares: ICA. ICA achieves substantially lower RMSE when c_{ICA} is small (coefficient cancellation regime).



(b) RMSE difference (ICA – higher-order OML) vs. ICA variance coefficient. Blue points indicate ICA outperforms higher-order OML; red points indicate higher-order OML outperforms ICA. The transition occurs around $c_{\text{ICA}} \approx 1.5$.

Figure E.6: Effect of the ICA variance coefficient on estimator performance.

Table E.2: **Randomized coefficient ablation across noise distributions.** ($n = 5,000$, 20 configs \times 20 replications each). Coefficients drawn from $a \in [-10, 10]$, $b \in [-0.5, 0.5]$, $\theta \in [0.001, 0.2]$.

Distribution	κ	OML RMSE	ICA RMSE	$ \Delta $ Bias	Winner
Discrete	4.97	0.0191	0.0148	0.4	ICA
Laplace	3.06	0.0362	0.0161	0.0	ICA
Gennorm ($\beta=4$)	-0.80	0.0292	0.0163	1.4	ICA
Uniform	-1.19	0.0172	0.0125	0.3	ICA
Rademacher	-2.00	0.0148	0.0127	0.2	ICA

E.4.5 Dependence on Treatment Effect Magnitude

Figure E.7 shows how performance varies with the treatment effect θ , with Tab. E.3 providing detailed statistics. Larger treatment effects tend to increase c_{ICA} (since $\|b + a\theta\|^2$ grows quadratically in θ when $a \neq 0$), which can degrade ICA’s relative performance. Additional visualizations are provided in Figs. E.8 and E.9, showing RMSE and bias differences across noise distributions and coefficient configurations.

Table E.3: **Performance by treatment effect magnitude.** (fixed coefficient ablation, 16 configurations per θ value).

θ	Avg. c_{ICA}	ICA Wins	Median RMSE Diff
0.01	1.62	12/16 (75%)	-0.0023
0.10	1.62	12/16 (75%)	-0.0018
0.50	1.73	12/16 (75%)	-0.0015
1.00	2.16	11/16 (69%)	-0.0008
3.00	7.15	11/16 (69%)	-0.0005
10.00	65.92	12/16 (75%)	-0.0012

E.5 SUMMARY

The coefficient ablation experiments reveal that ICA’s performance is governed by the ICA variance coefficient $c_{ICA} = 1 + \|b + a\theta\|_2^2$:

- When coefficients nearly cancel ($c_{ICA} \approx 1$), ICA achieves substantially lower variance than higher-order OML.
- The transition region $c_{ICA} \in [1.5, 5]$ marks where higher-order OML becomes competitive.
- Higher-order OML exhibits more stable performance across configurations (std = 0.0031) compared to ICA (std = 0.0076).
- The treatment effect magnitude affects c_{ICA} quadratically, but ICA remains competitive across the tested range.

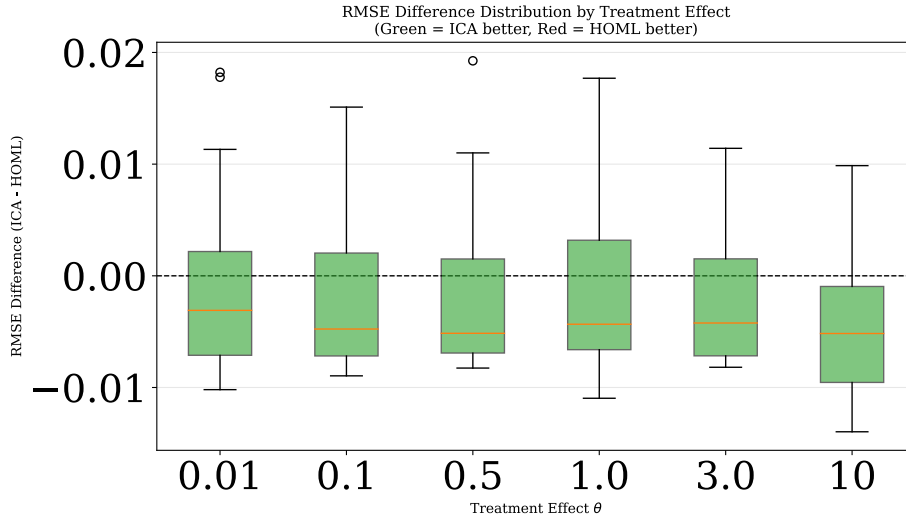


Figure E.7: **Box plots of RMSE difference (ICA – higher-order OML) by treatment effect.** Negative values indicate ICA advantage. The median difference remains negative across all treatment effect values.

E.6 NONLINEAR PLR ABLATIONS

These figures provide additional details for the nonlinear PLR experiments in § 4.2.

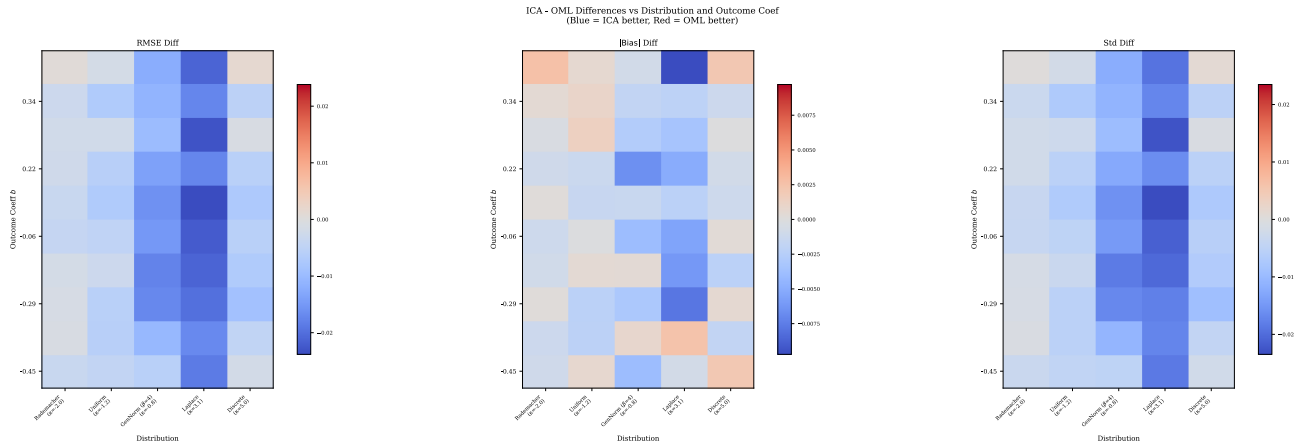


Figure E.8: **Combined heatmap showing RMSE, bias, and standard deviation differences across all randomized coefficient configurations.** Organized by treatment noise distribution η and outcome coefficient bin.

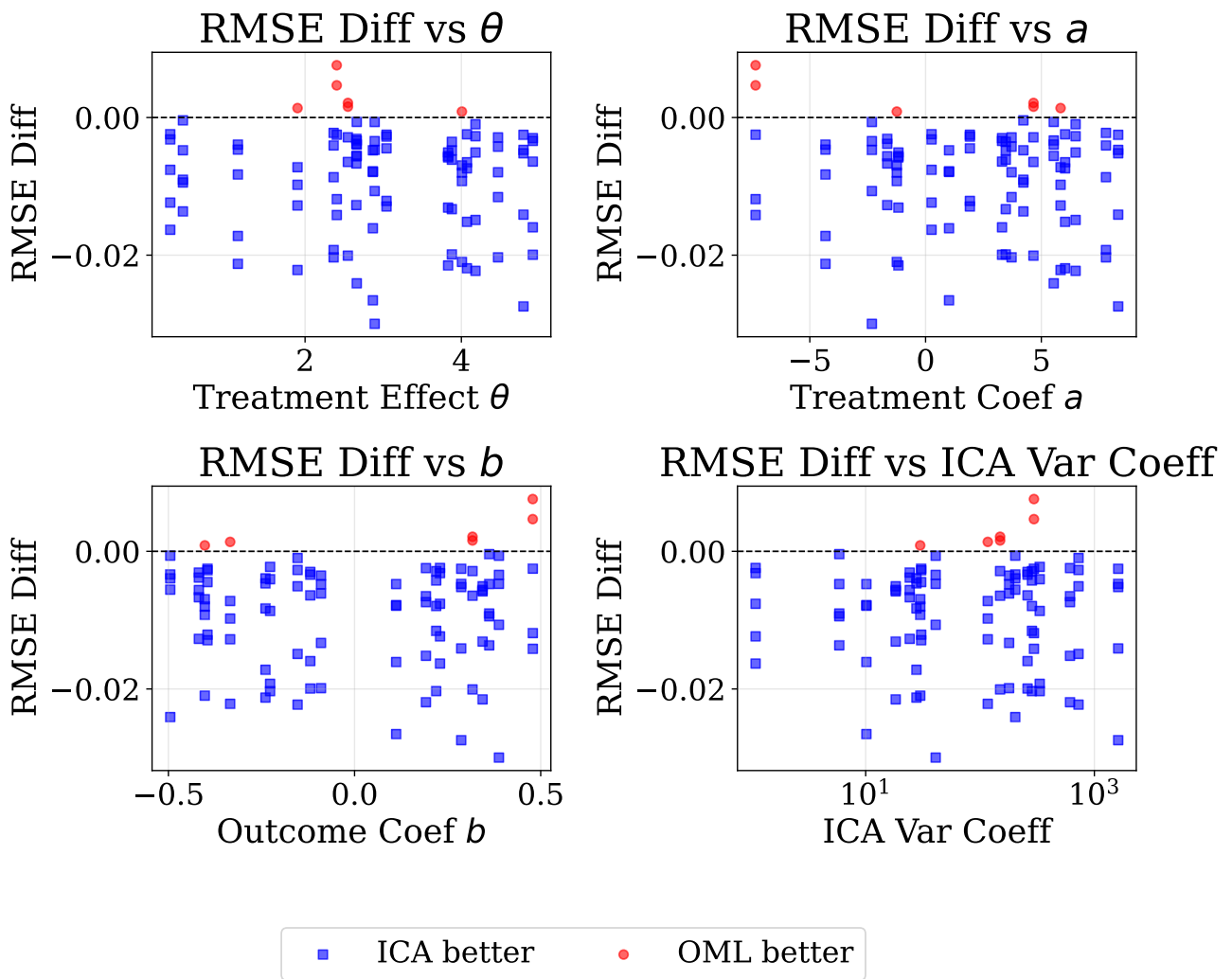


Figure E.9: **RMSE difference grid for randomized coefficients.** ($a \in [-10, 10]$, $b \in [-0.5, 0.5]$, $\theta \in [0, 5]$). Each panel shows RMSE difference vs. a different variable: treatment effect θ (top-left), treatment coefficient a (top-right), outcome coefficient b (bottom-left), and ICA variance coefficient (bottom-right). Blue: ICA better; red: higher-order OML better.

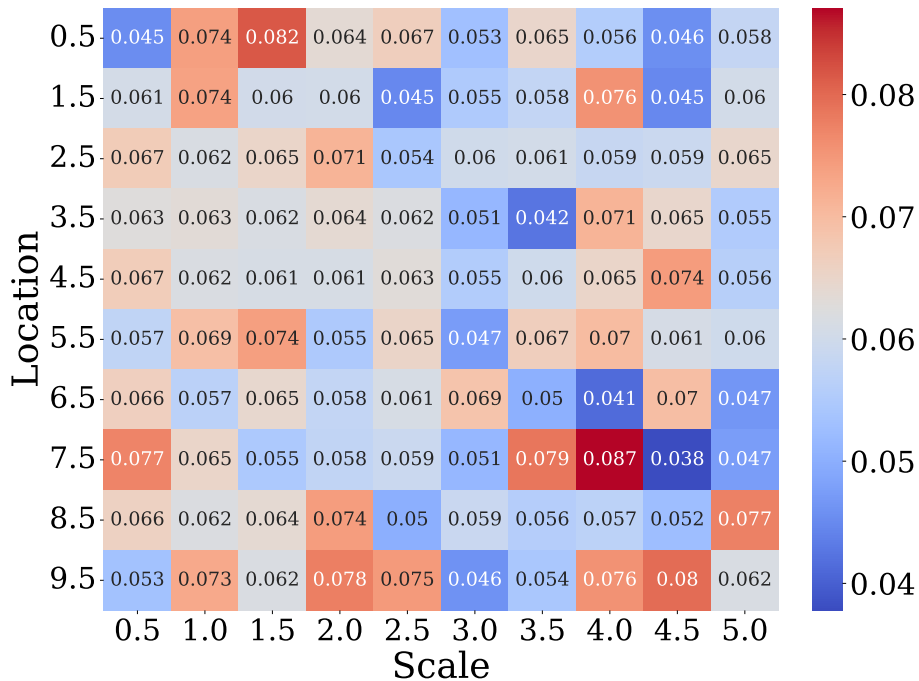


Figure E.10: **Effect of location-scale transformation on treatment effect estimation in nonlinear PLR.** Shows MSE across different transformation parameters.

E.7 MULTIPLE TREATMENT ABLATIONS

These figures provide additional details for the multiple treatment experiments in § 4.3.

E.8 FASTICA ABLATIONS

FastICA loss function. Fig. E.16 compares FastICA loss functions for treatment effect estimation. The `logcosh` loss outperforms `cube` (which corresponds to optimizing for excess kurtosis) and matches `exp`, motivating our default choice. Settings: $\theta = 1.55$, $d = 50$, single treatment, $n = 5,000$, Laplace covariates ($\beta = 1$), coefficients drawn from $\mathcal{N}(0, 1)$ with 30% sparsity (≈ 15 non-zeros out of $d = 50$), averaged over 20 seeds.

Sparsity of the DGP. We investigate how sparsity of the coefficient matrix \mathbf{A} (covariate \rightarrow treatment) affects estimation. Sparsity is controlled via Bernoulli masking probability. Fig. E.17 shows MSE remains stable across sparsity levels; we use 0.4 throughout. Settings: $d = 50$, single treatment, $n = 5,000$, 20 seeds. Additionally, Fig. E.14 examines the effect of Gaussian covariates versus Laplace noise and different treatment effect sampling strategies on relative MSE.

E.9 FASTICA VS. DIRECTLINGAM COMPARISON

We conduct systematic comparisons between FastICA and DirectLiNGAM [Shimizu et al., 2011] for causal treatment effect estimation. While both methods exploit non-Gaussianity for identification, they differ fundamentally: FastICA performs blind source separation to recover independent components, whereas DirectLiNGAM directly estimates the causal graph structure via recursive regression and independence testing.

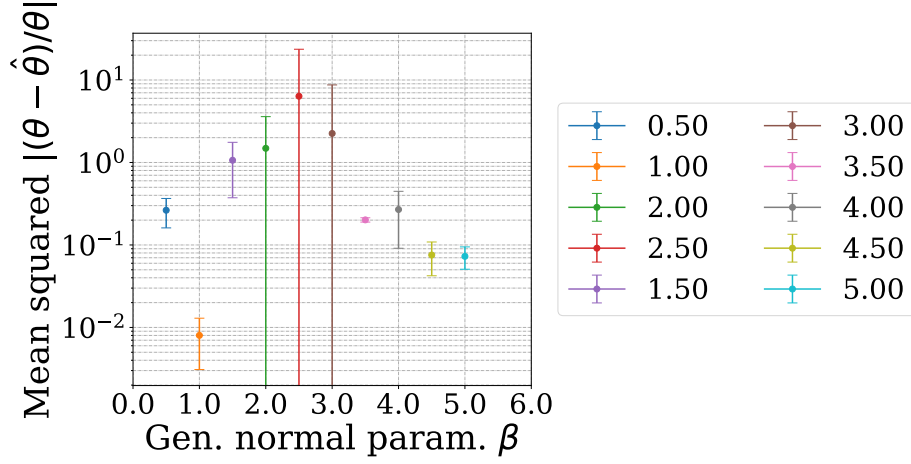


Figure E.11: **MSE vs. distribution shape parameter β in nonlinear PLR.** Shows performance across generalized normal distributions with varying tail heaviness.

E.9.1 Data Generating Process

We generate data according to a nonlinear structural equation model:

$$X_i = S_i, \quad i = 1, \dots, d, \quad (41)$$

$$T_j = S_{d+j} + \sum_{i=1}^d A_{ji} \cdot \sigma(X_i), \quad j = 1, \dots, k, \quad (42)$$

$$Y = S_{d+k+1} + \sum_{j=1}^k \theta_j T_j + \sum_{i=1}^d B_i \cdot \sigma(X_i), \quad (43)$$

where $S \in \mathbb{R}^{d+k+1}$ are mutually independent source signals drawn from a generalized normal distribution with shape parameter β , $\sigma(\cdot)$ denotes the leaky ReLU activation function, and $A \in \mathbb{R}^{k \times d}$ is a sparse coefficient matrix with sparsity controlled by probability p_{sparse} . The treatment effects $\theta = (1.55, 0.65, -2.45, 1.75, -1.35)^\top$ are fixed across experiments.

E.9.2 Experimental Design

We compare FastICA and DirectLiNGAM across five experimental dimensions, each with 20 random seeds for statistical stability:

1. **Sparsity:** $p_{\text{sparse}} \in \{0.0, 0.1, \dots, 0.9\}$ with $n = 5,000$, $d = 50$, $k = 1$
2. **Distribution shape:** $\beta \in \{0.5, 1.0, \dots, 5.0\}$ with $n = 200$, $d = 10$, $k = 1$
3. **Sample size:** $n \in \{100, 200, 500, 1000, 2000, 5000\}$ with $d = 10$, $k = 1$
4. **Covariate dimension:** $d \in \{2, 5, 10, 20, 50\}$ with $n = 1,000$, $k = 1$
5. **Number of treatments:** $k \in \{1, 2, 3, 4, 5\}$ with $n = 1,000$, $d = 10$

E.9.3 Results: FastICA vs. DirectLiNGAM Comparison

Results: Sparsity Ablation Table E.4 and Fig. E.18 present results across sparsity levels. DirectLiNGAM achieves substantially lower MSE for dense models ($p_{\text{sparse}} \leq 0.4$), with up to $4.7\times$ improvement at $p_{\text{sparse}} = 0$. However, FastICA becomes competitive for sparse models ($p_{\text{sparse}} \geq 0.5$), achieving lower MSE while being approximately $270\times$ faster on average (0.56s vs. 151.8s).

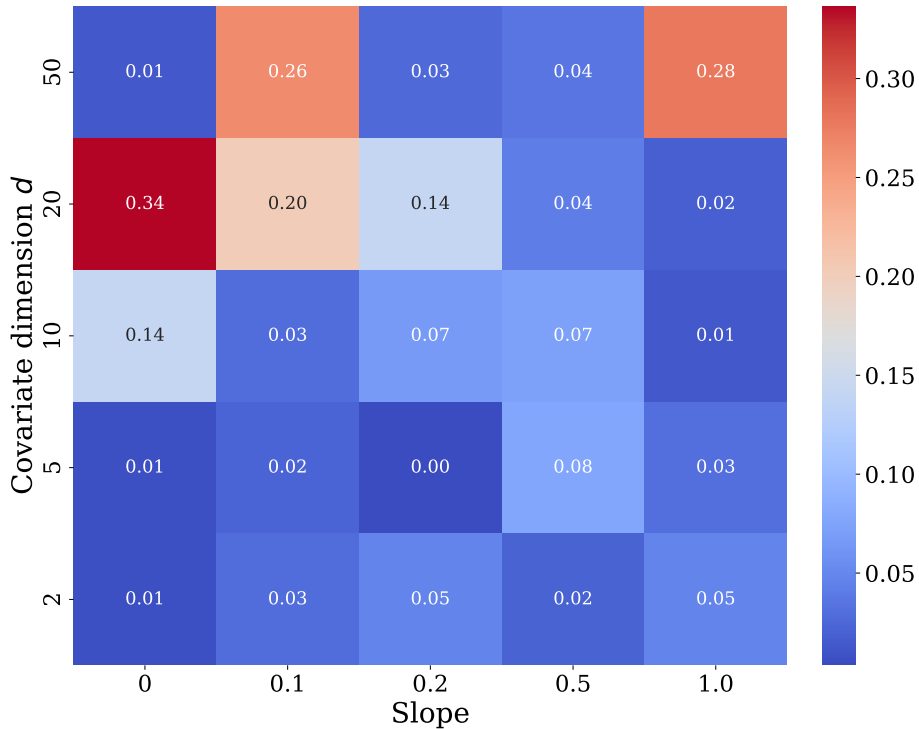


Figure E.12: **Effect of leaky ReLU slope and covariate dimension on treatment effect estimation.** Shows MSE heatmap across different nonlinearity strengths and dimensionalities.

Results: Dimensionality Scaling The relative performance depends critically on the covariate dimension d (Table E.5 and Fig. E.19). DirectLiNGAM dominates for low-dimensional settings ($d \leq 10$), achieving up to $2.7\times$ lower MSE at $d = 2$. However, FastICA becomes preferable for high-dimensional data ($d \geq 20$), where DirectLiNGAM’s MSE degrades while its runtime increases dramatically (35.5s at $d = 50$ vs. 0.22s for FastICA).

Results: Distribution Shape, Sample Size, and Multiple Treatments Three additional ablations show broadly consistent patterns (Tab. E.6). Across all tested **sample sizes** ($n \in \{100, \dots, 5,000\}$) and **number of treatments** ($k \in \{1, \dots, 5\}$), DirectLiNGAM uniformly achieves $2\text{--}2.4\times$ lower MSE than FastICA with moderate runtime overhead ($3\text{--}4\times$ slower). For **distribution shape** ($\beta \in \{0.5, \dots, 5.0\}$), FastICA wins only for heavily non-Gaussian sources ($\beta = 0.5$, MSE 0.052 vs. 0.120); DirectLiNGAM dominates for all $\beta \geq 1$.

Table E.4: **FastICA vs. DirectLiNGAM across sparsity levels.** ($n = 5,000$, $d = 50$, $k = 1, 20$ seeds).

p_{sparse}	MSE		Runtime (s)		Winner
	FastICA	DirectLiNGAM	FastICA	DirectLiNGAM	
0.0	0.064	0.014	1.40	365.5	DirectLiNGAM
0.1	0.091	0.034	1.08	359.1	DirectLiNGAM
0.2	0.085	0.076	0.94	277.3	DirectLiNGAM
0.3	0.114	0.068	0.40	149.7	DirectLiNGAM
0.4	0.122	0.100	0.37	78.6	DirectLiNGAM
0.5	0.085	0.118	0.42	61.6	FastICA
0.6	0.085	0.154	0.39	62.8	FastICA
0.7	0.109	0.148	0.18	52.3	FastICA
0.8	0.102	0.148	0.19	55.4	FastICA
0.9	0.079	0.154	0.22	55.7	FastICA

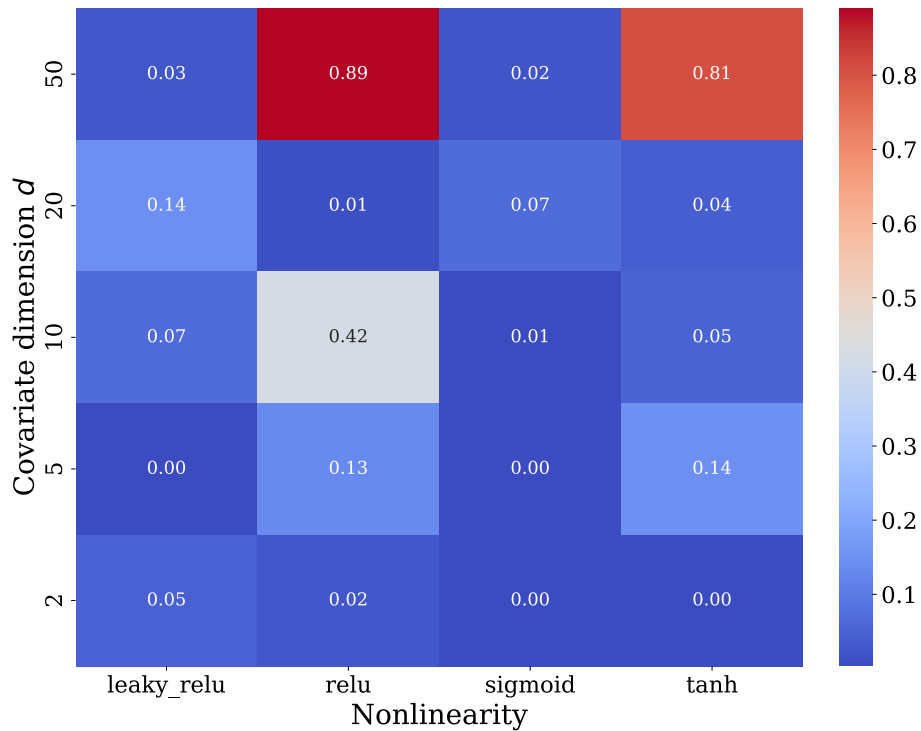


Figure E.13: **Robustness across covariate dimensions and nonlinearity types.** Shows relative MSE of treatment effect estimation for linear ICA across different covariate dimensions and nonlinear transformations in the PLR model.

Table E.5: **FastICA vs. DirectLiNGAM across covariate dimensions.** ($n = 1,000$, $k = 1, 20$ seeds).

d	MSE		Runtime (s)		Winner
	FastICA	DirectLiNGAM	FastICA	DirectLiNGAM	
2	0.037	0.014	0.007	0.027	DirectLiNGAM
5	0.059	0.014	0.006	0.101	DirectLiNGAM
10	0.061	0.024	0.012	0.567	DirectLiNGAM
20	0.082	0.086	0.032	2.852	FastICA
50	0.144	0.231	0.224	35.524	FastICA

E.10 SUMMARY

Our comprehensive comparison reveals complementary strengths:

- **DirectLiNGAM** achieves superior accuracy for low-dimensional, dense, moderately non-Gaussian settings, but scales poorly with dimension ($O(d^3)$ complexity).
- **FastICA** excels for sparse, high-dimensional, or heavily non-Gaussian data, with consistent sub-second runtime regardless of problem structure.
- The crossover point occurs around $d \approx 15$ – 20 covariates or $p_{\text{sparse}} \approx 0.5$ sparsity.

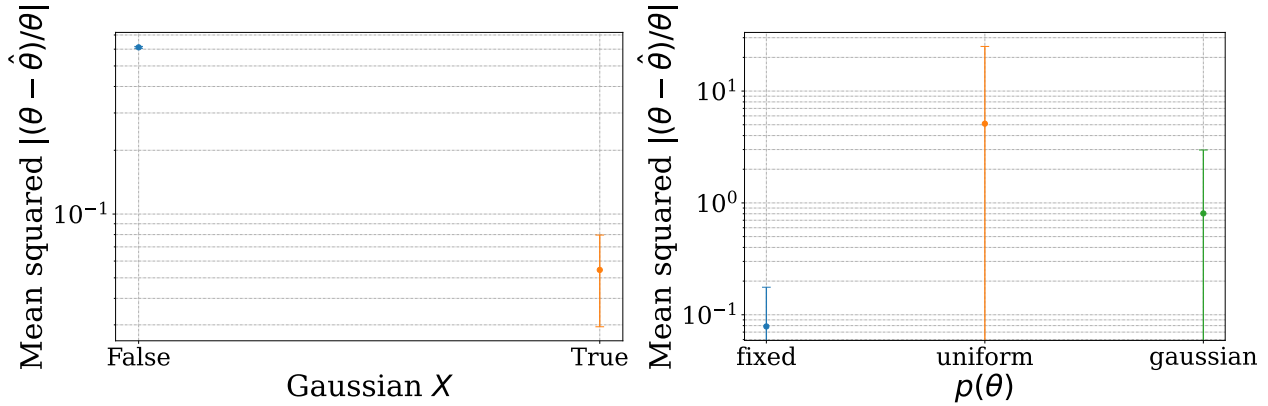


Figure E.14: **Effect of (Left) Gaussian covariates and (Right) treatment effect sampling on relative MSE with linear ICA in nonlinear PLR.** Mean \pm std from 20 seeds. Left: “true” = Gaussian X , Laplace T, Y . Right: “fixed” = $\theta = 1.55$; “uniform” = $\theta \sim U[0, 1]$; “normal” = $\theta \sim \mathcal{N}(0, 1)$.

Table E.6: **Summary of three ablations where DirectLiNGAM wins broadly.** Ranges report (min, max) MSE across the swept parameter; $k = 1$ and $\beta = 1$ unless swept. All experiments use 20 seeds.

Ablation	Swept range	FastICA MSE	DirectLiNGAM MSE	Winner
Distribution (β)	0.5–5.0	0.052–1.863	0.106–0.506	Mixed*
Sample size (n)	100–5,000	0.031–0.596	0.014–0.249	DirectLiNGAM
Treatments (k)	1–5	0.054–0.161	0.033–0.079	DirectLiNGAM

*FastICA wins only at $\beta = 0.5$ (heavy-tailed); DirectLiNGAM dominates for $\beta \geq 1$.

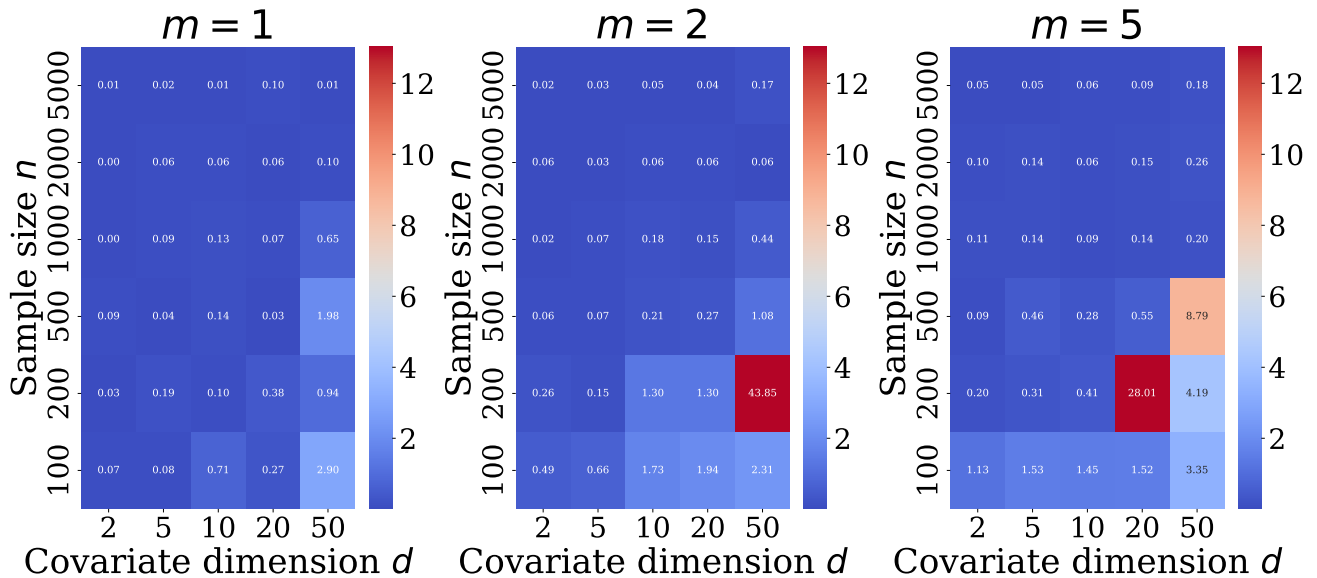


Figure E.15: **ICA relative MSE: covariate dimension vs. sample size for $m \in \{1, 2, 5\}$ treatments.** Each panel shows the mean relative MSE of the ICA treatment effect estimate across 20 seeds. The shared colorscale is clipped to the 2nd–98th percentile for readability (the outlier at $d=50, n=200, m=2$ reaches ≈ 44). Settings: Laplace covariates ($\beta = 1$), 30% sparsity in the mixing matrix.

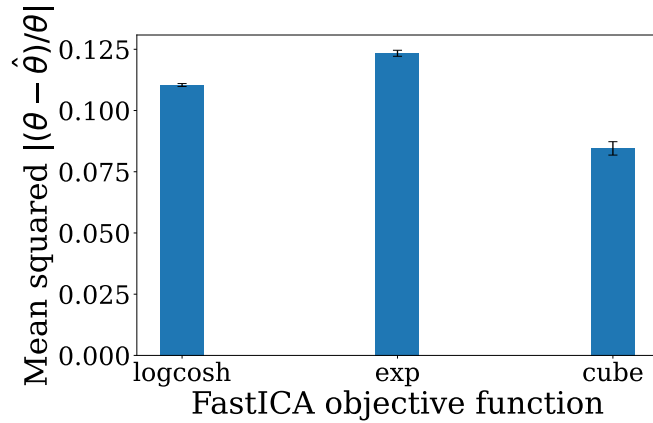


Figure E.16: MSE across FastICA loss functions. ($d = 50, n = 5,000$, single treatment). Mean \pm std from 20 seeds.

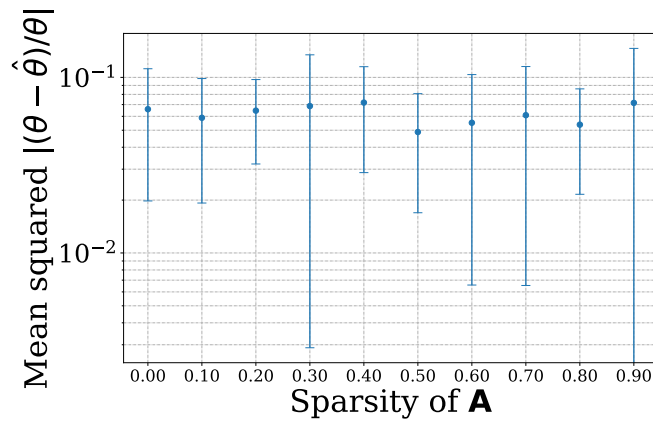


Figure E.17: MSE vs. sparsity of $\mathbf{A} : X \rightarrow T$. ($d = 50, n = 5,000$). Mean \pm std from 20 seeds.

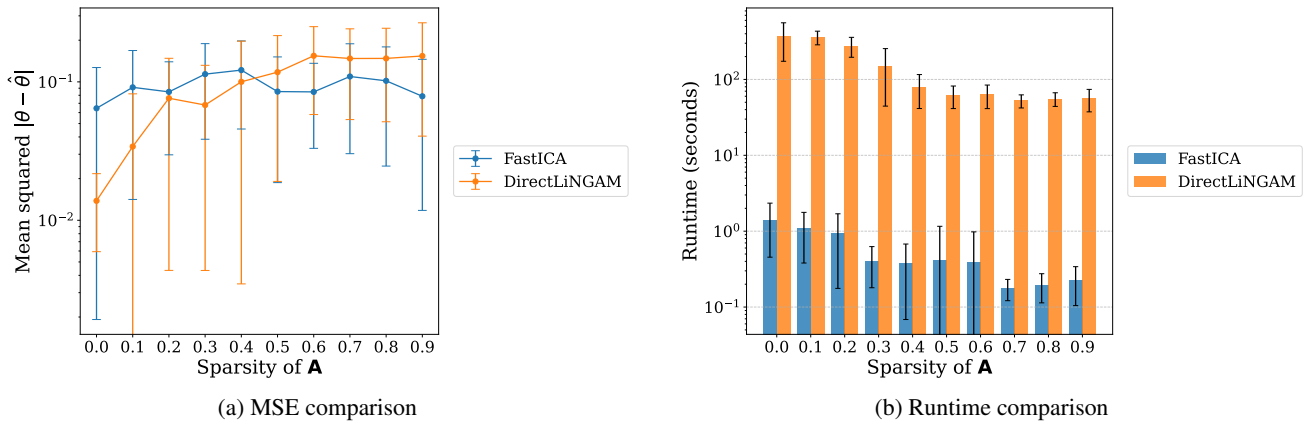
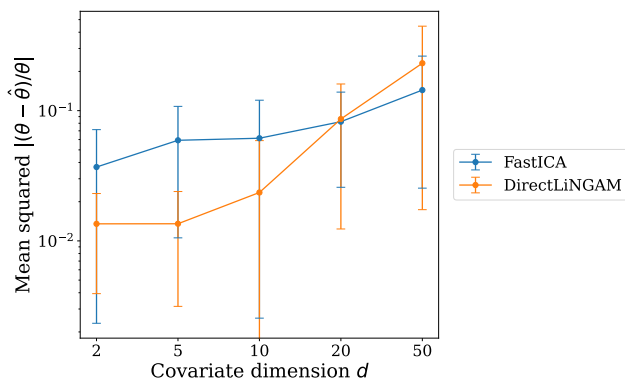
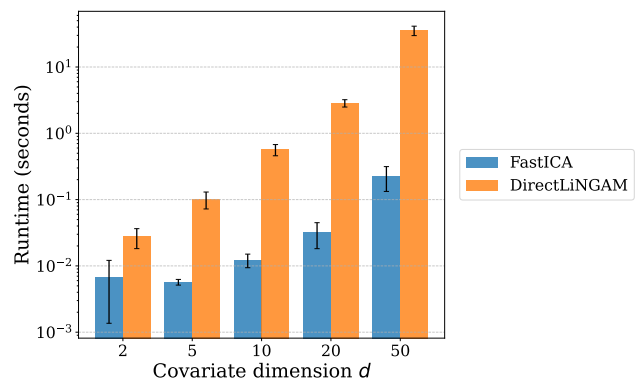


Figure E.18: **FastICA vs. DirectLiNGAM across sparsity levels.** ($n = 5,000, d = 50$). (a) Mean squared error with standard error bars. DirectLiNGAM dominates for dense models ($p_{\text{sparse}} \leq 0.4$); FastICA excels for sparse models. (b) Runtime comparison showing DirectLiNGAM's significant computational overhead.



(a) MSE vs. dimension



(b) Runtime vs. dimension

Figure E.19: **FastICA vs. DirectLiNGAM across covariate dimensions.** ($n = 1,000, k = 1$). (a) DirectLiNGAM dominates for $d \leq 10$; FastICA becomes preferable for $d \geq 20$. (b) DirectLiNGAM runtime scales cubically with dimension.